Article

Molecular Cell

c-di-GMP Arms an Anti-σ to Control Progression of Multicellular Differentiation in *Streptomyces*

Graphical Abstract

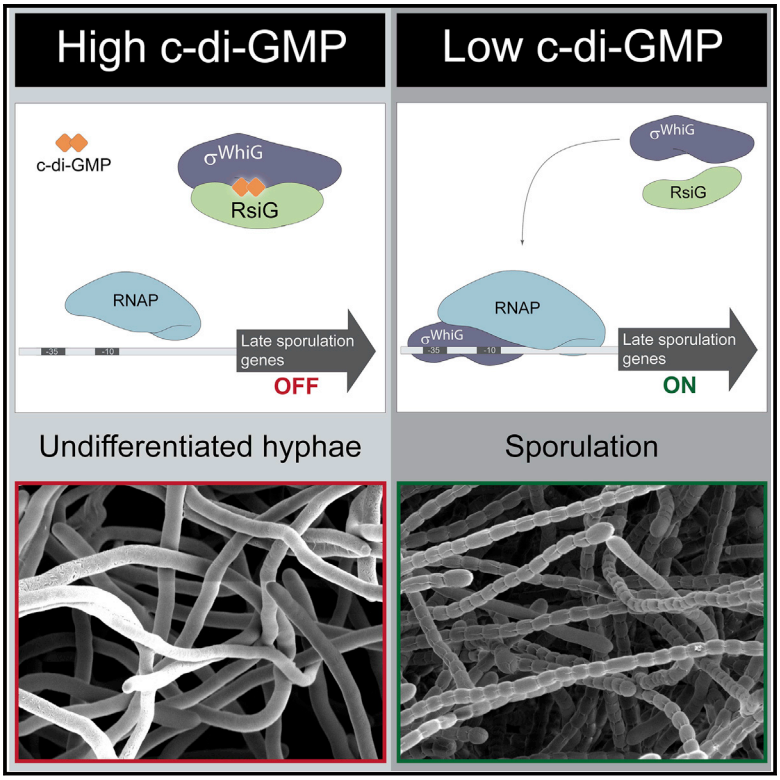

Authors

Kelley A. Gallagher, Maria A. Schumacher, Matthew J. Bush, ..., Kim C. Findlay, Richard G. Brennan, Mark J. Buttner

Correspondence

maria.schumacher@duke.edu (M.A.S.), mark.buttner@jic.ac.uk (M.J.B.)

In Brief

In the antibiotic-producing bacterium *Streptomyces*, an unusual dimer of the cyclic dinucleotide signaling molecule c-di-GMP mediates effective complex formation between a sporulation-specific σ and its cognate anti-σ to control differentiation of the reproductive hyphae into spores. The anti-σ binds c-di-GMP using two copies of a novel $E(X)_3S(X)_2R(X)_3Q(X)_3D$ signature motif.

Highlights

- c-di-GMP controls development in the multicellular bacterium *Streptomyces*
- c-di-GMP mediates complex formation between sporulation σ, σ^{WhiG}, and anti-σ, RsiG
- RsiG uses two novel $E(X)_3S(X)_2R(X)_3Q(X)_3D$ signature motifs to bind two c-di-GMPs
- When c-di-GMP levels drop, σ^{WhiG} is released to activate late sporulation regulators

Gallagher et al., 2020, Molecular Cell 77, 586–599
February 6, 2020
https://doi.org/10.1016/j.molcel.2019.11.006

CellPress

CellPress

Molecular Cell
Article

c-di-GMP Arms an Anti-σ to Control Progression of Multicellular Differentiation in *Streptomyces*

Kelley A. Gallagher,[1,4,5] Maria A. Schumacher,[2,5,*] Matthew J. Bush,[1] Maureen J. Bibb,[1] Govind Chandra,[1] Neil A. Holmes,[1] Wenjie Zeng,[2] Max Henderson,[2] Hengshan Zhang,[2] Kim C. Findlay,[3] Richard G. Brennan,[2] and Mark J. Buttner[1,6,*]

[1]Department of Molecular Microbiology, John Innes Centre, Norwich Research Park, Norwich NR4 7UH, UK
[2]Department of Biochemistry, Duke University School of Medicine, Durham, NC 27710, USA
[3]Department of Cell and Developmental Biology, John Innes Centre, Norwich Research Park, Norwich NR4 7UH, UK
[4]Present address: Département de Microbiologie, Infectiologie et Immunologie, Université de Montréal, Montréal, QC H3T 1J4, Canada
[5]These authors contributed equally to this work
[6]Lead Contact
*Correspondence: maria.schumacher@duke.edu (M.A.S.), mark.buttner@jic.ac.uk (M.J.B.)
https://doi.org/10.1016/j.molcel.2019.11.006

SUMMARY

Streptomyces **are our primary source of antibiotics, produced concomitantly with the transition from vegetative growth to sporulation in a complex developmental life cycle. We previously showed that the signaling molecule c-di-GMP binds BldD, a master repressor, to control initiation of development. Here we demonstrate that c-di-GMP also intervenes later in development to control differentiation of the reproductive hyphae into spores by arming a novel anti-σ (RsiG) to bind and sequester a sporulation-specific σ factor (σ^{WhiG}). We present the structure of the RsiG-(c-di-GMP)$_2$-σ^{WhiG} complex, revealing an unusual, partially intercalated c-di-GMP dimer bound at the RsiG-σ^{WhiG} interface. RsiG binds c-di-GMP in the absence of σ^{WhiG}, employing a novel $E(X)_3S(X)_2R(X)_3Q(X)_3D$ motif repeated on each helix of a coiled coil. Further studies demonstrate that c-di-GMP is essential for RsiG to inhibit σ^{WhiG}. These findings reveal a newly described control mechanism for σ-anti-σ complex formation and establish c-di-GMP as the central integrator of** ***Streptomyces*** **development.**

INTRODUCTION

Nucleotide second messengers are crucial intracellular signals in all domains of life. In bacteria, one of the most widespread nucleotide second messengers is 3′,5′-cyclic diguanylic acid (c-di-GMP), which regulates diverse global cellular processes that allow bacteria to respond rapidly to dynamic environmental conditions (Jenal et al., 2017). Levels of intracellular c-di-GMP are determined by the action of diguanylate cyclases (DGCs), which are characterized by active site GGDEF motifs that synthesize c-di-GMP from two molecules of GTP (Paul et al., 2004; Chan et al., 2004) and by c-di-GMP hydrolyzing phosphodiesterases (PDEs), characterized by EAL or HD-GYP domains (Schmidt et al., 2005; Christen et al., 2005; Ryan et al., 2017). DGCs and PDEs are often associated with sensory domains, which allow the cell to adjust c-di-GMP levels in direct response to specific environmental stimuli (Hengge, 2009).

Although DGCs and PDEs conform to a few well-conserved structural classes (Schirmer and Jenal, 2009; Lovering et al., 2011) and can be identified bioinformatically, the downstream targets of c-di-GMP signaling are structurally diverse, with multiple protein and RNA folds shown to bind c-di-GMP (Chou and Galperin, 2016). The first c-di-GMP-binding effectors to be identified included degenerate (non-catalytic) GGDEF or EAL proteins (Newell et al., 2009, 2011; Duerig et al., 2009; Lee et al., 2007; Qi et al., 2011), c-di-GMP-specific GEMM riboswitches (Sudarsan et al., 2008), and the PilZ domain (Amikam and Galperin, 2006; Ryjenkov et al., 2006), which is involved in the regulation of a wide range of cellular processes, including motility in *E. coli* (Boehm et al., 2010) and cellulose synthesis in *Komagataeibacter xylinus* (formerly *Acetobacter xylinum*), the system where c-di-GMP was first discovered (Ross et al., 1987; Morgan et al., 2014). Subsequent biochemical screens for c-di-GMP-binding effectors have identified the ATPase domains of functionally diverse proteins (Lori et al., 2015; Trampari et al., 2015; Roelofs et al., 2015; Matsuyama et al., 2016), a membrane transporter (Steiner et al., 2013), a histidine kinase (Dubey et al., 2016), and the ribosome-modifying enzyme RimK (Little et al., 2016).

Transcription factors represent a particularly varied subset of c-di-GMP effector proteins and include Crp family members (Leduc and Roberts, 2009; Chin et al., 2010; Fazli et al., 2011), TetR-like proteins (Li and He, 2012; Li et al., 2018a, 2018b), the NtrC-like protein VspR from *Vibrio cholerae* (Srivastava et al., 2011), and AAA+ ATPases (Baraquet and Harwood, 2013; Srivastava et al., 2013; Skotnicka et al., 2016; Matsuyama et al., 2016). The diverse c-di-GMP-responsive transcription factors for which structural information is available and c-di-GMP binding is understood include VpsT, which is a member of the FixJ/LuxR/CsgD family of response regulators (Krasteva et al., 2010); the AAA+ ATPase enhancer-binding protein FleQ, which acts as a master regulator of flagellar motility in *Pseudomonas* (Matsuyama et al., 2016); *K. pneumoniae* MrkH, a PilZ transcription regulator of biofilm formation (Schumacher and Zeng, 2016; Wang et al., 2016); the MerR family member BrlR (Chambers

et al., 2014; Raju and Sharma, 2017); and BldD, the master regulator of development in *Streptomyces* (Tschowri et al., 2014). There is no significant conservation between the c-di-GMP binding motifs found in different c-di-GMP effector proteins, rendering bioinformatic identification not possible. As a result, new c-di-GMP effectors, most notably transcription regulators, must be identified experimentally.

In Gram-negative bacteria, the responses mediated by cellular c-di-GMP levels include virulence, motility, and biofilm formation (Jenal et al., 2017). In contrast, less is known about the role of c-di-GMP in Gram-positive bacteria. However, we recently showed that, in the filamentous Gram-positive bacteria *Streptomyces*, c-di-GMP controls initiation of development (Tschowri et al., 2014; Bush et al., 2015). *Streptomyces* are ubiquitous, primarily soil-dwelling bacteria with a complicated developmental life cycle involving progression from vegetative growth to production of reproductive aerial hyphae that differentiate into chains of exospores (Flärdh and Buttner, 2009; Flärdh et al., 2012; McCormick and Flärdh, 2012; Bush et al., 2015). Entry into development coincides with biosynthesis of numerous secondary metabolites that serve as our most abundant source of clinically important antibiotics and provide other medically important drugs, such as anticancer agents and immunosuppressants (Hopwood, 2007; Liu et al., 2013; van Wezel and McDowall, 2011). Consequently, there is considerable interest in understanding the mechanisms that control this developmental transition. The controlling transcription factors of the *Streptomyces* sporulation regulatory network are encoded by the *bld* and the *whi* loci (Flärdh and Buttner, 2009; Flärdh et al., 2012; McCormick and Flärdh, 2012; Bush et al., 2015). Mutations in *bld* genes prevent production of reproductive aerial hyphae, resulting in ''bald'' colonies lacking the fuzzy appearance of the wild type (WT). Mutations in *whi* genes prevent reproductive aerial hyphae differentiating into mature spore chains, producing ''white'' colonies because they fail to synthesize the green polyketide pigment associated with fully developed spores.

The dramatic phenotypic consequences of altered c-di-GMP levels in *Streptomyces*, where high c-di-GMP levels trap the bacteria in vegetative growth and low c-di-GMP levels cause precocious hypersporulation (Tschowri et al., 2014; Tschowri, 2016; Al-Bassam et al., 2018; den Hengst et al., 2010; Tran et al., 2011; Hull et al., 2012; Bush et al., 2015; Latoscha et al., 2019), suggested that this signaling molecule must directly interact with the regulatory network controlling the life cycle. In 2014, a direct link between c-di-GMP and the regulatory cascade was established with the discovery that the master regulator BldD is a c-di-GMP effector protein (Tschowri et al., 2014). BldD is a repressor that sits at the top of the developmental regulatory network, serving to repress a large set of genes, including many genes of the core transcriptional regulatory cascade itself (den Hengst et al., 2010; Tschowri et al., 2014; Bush et al., 2015). Structural and biochemical analyses showed that BldD dimerization and, hence, its ability to bind DNA depends on the binding of a novel tetrameric form of c-di-GMP to the C-terminal domain (CTD) of the protein (Tschowri et al., 2014; Schumacher et al., 2017).

These data showed that BldD-c-di-GMP controls the onset of development. By contrast, what controls the final stage of development, differentiation of the reproductive aerial hyphae into spores, has been unknown. The sporulation-specific σ factor σ^{WhiG} is known to play a key role in this stage of development (Flärdh et al., 1999; Chater et al., 1989), but its function has not been subjected to systematic analysis. Here we identify a novel anti-σ factor, RsiG, that controls the activity of σ^{WhiG}. Strikingly, we show that the interaction between RsiG and σ^{WhiG} is mediated by c-di-GMP. Specifically, when ''armed'' with a dimer of c-di-GMP, RsiG sequesters σ^{WhiG}, blocking differentiation of the reproductive hyphae into spores. This is the first known instance of c-di-GMP targeting a σ factor. Thus, like BldD, the RsiG-σ^{WhiG} complex senses changes in c-di-GMP levels to control a specific stage of development. In this complex, RsiG primarily binds the cyclic dinucleotide via two $E(X)_3S(X)_2R(X)_3Q(X)_3D$ signatures, one on each helix of its antiparallel coiled coil. This signature is distinct from any previously observed c-di-GMP binding motif. Notably, the anti-σ factor RsiG can bind c-di-GMP in the absence of σ^{WhiG}, and that binding is specific for this nucleotide. We also show that RsiG must bind c-di-GMP to carry out its function of inhibiting σ^{WhiG} activity during vegetative growth, preventing premature expression of the σ^{WhiG} regulon. Conservation of the signature c-di-GMP binding motifs in all *Streptomyces* RsiG homologs suggests that regulation of RsiG-σ^{WhiG} complex formation by this second messenger is a general mechanism of developmental control across the genus.

RESULTS

σ^{WhiG} Levels Are Critical to the Developmental Fate of Hyphae in *Streptomyces venezuelae*

One factor known to be important in the later stages of *Streptomyces* development is the sporulation-specific σ factor σ^{WhiG}. In particular, this σ factor has been shown previously to play a key role in the differentiation of reproductive hyphae into spores in the classical model species *Streptomyces coelicolor* (Flärdh et al., 1999; Chater et al., 1989), but its function had not been subjected to systematic analysis. Thus, to interrogate the function of σ^{WhiG}, we first examined the phenotypes associated with deletion and overexpression of *whiG* in *Streptomyces venezuelae*. We adopted *S. venezuelae* as a new model species to interrogate development because, unlike *S. coelicolor*, which differentiates only on plates, *S. venezuelae* also sporulates in a liquid medium (Bush et al., 2015; Schlimpert et al., 2016). A constructed *ΔwhiG* null mutant was unable to synthesize the green polyketide spore pigment associated with WT *S. venezuelae* spores, resulting in a classic white phenotype (Figure 1A). In *S. coelicolor*, *ΔwhiG* mutants fail to initiate sporulation septation, producing undifferentiated aerial hyphae (Flärdh et al., 1999; Chater et al., 1989), but the equivalent *S. venezuelae ΔwhiG* mutant showed an oligosporogenous phenotype, producing a mixture of undifferentiated aerial hyphae and occasional immature spore chains (Figure 1B). Conversely, overexpressing *whiG* in *S. venezuelae* using a strong constitutive promoter (*ermE**) caused a hypersporulation phenotype in which the vegetative hyphae differentiated into spore chains. As a consequence, the biomass of the resulting mature colonies consisted almost entirely of spores (Figure 1B), and the colonies appeared

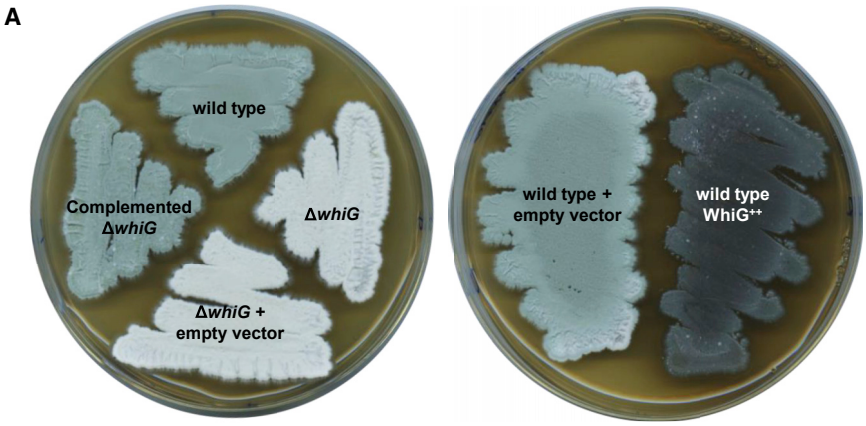

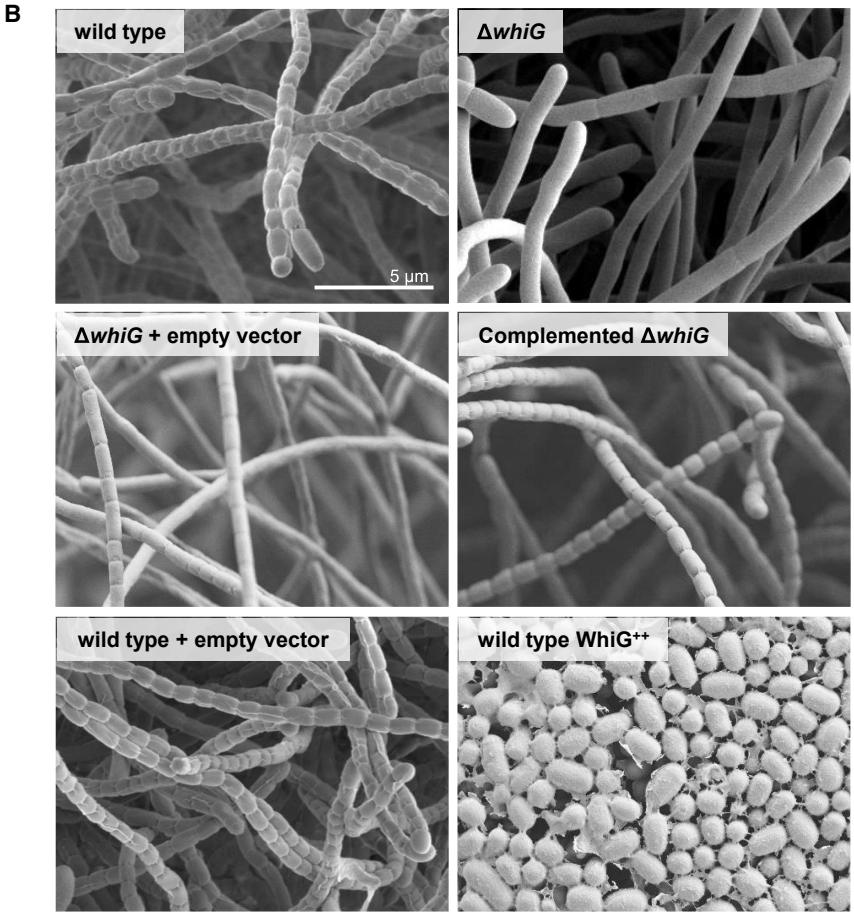

Figure 1. Overexpression of *whiG* Causes Hypersporulation on Solid Medium

(A) The phenotypes of WT *S. venezuelae*, the *whiG* mutant, the complemented *whiG* mutant, WT *S. venezuelae* overexpressing *whiG*, and strains carrying the corresponding empty vectors, photographed after 4 days of growth on Mannitol Yeast Extract Malt Extract (MYM) medium.

(B) Scanning electron micrographs of the same strains imaged after 4 days of growth on MYM medium.

See also Figure S1 and Video S2 for the effect of overexpressing *whiG* on sporulation in liquid culture.

bald to the naked eye because aerial mycelium formation had been bypassed. This hypersporulation phenotype was equally apparent in time-lapse images of the *whiG* overexpression strain differentiating in a microfluidic device (see below).

σ^{WhiG} Functions to Activate Transcription of *whiH* and *whiI*

To identify genes that are directly activated by σ^{WhiG}, we used a combination of genome-wide σ^{WhiG} chromatin immunoprecipitation sequencing (ChIP-seq) and transcriptional profiling of WT *S. venezuelae* and the *ΔwhiG* mutant. We found that σ^{WhiG} controls three target genes: the key late developmental regulatory genes *whiH* (*vnz27205*) and *whiI* (*vnz28820*), which have been identified previously as σ^{WhiG} targets in *S. coelicolor* (Ryding et al., 1998; Aínsa et al., 1999), and a third gene encoding a membrane protein of unknown function (*vnz15005*) (Figure 2). Time-resolved transcription profiling of differentiating cultures of WT *S. venezuelae* and the *whiG* null mutant showed that expression of *whiI* and *vnz15005* depends completely on *whiG*, whereas expression of *whiH* is partially dependent on *whiG* (Figure 2B). Despite its role in controlling sporulation in *Streptomyces*, phylogenetically σ^{WhiG} belongs to a clade of σ factors that control flagellum biosynthesis in diverse motile bacteria, including σ^{28} (also called σ^{FliA}) in enteric bacteria and σ^{D} in *Bacillus subtilis* (Chater et al., 1989; Hughes et al., 1993; Helmann and Chamberlin, 1987). The −10 and −35 promoter sequences of *S. venezuelae whiH*, *whiI*, and *vnz15005* (Figure 2C) show clear similarity to the consensus sequences of these true flagellar σ factors.

A mutant deleted for the uncharacterized σ^{WhiG} target gene, *vnz15005*, had no detectable phenotype. In addition, although *whiH* and *whiI* are present in more than 98% of the 802 complete and annotated *Streptomyces* genomes available at GenBank (https://www.ncbi.nlm.nih.gov/genbank/), homologs of *vnz15005* are present in only 34%. These results suggest that the main function of σ^{WhiG} is to activate expression of *whiH* and *whiI*. To test this hypothesis, we placed *whiH* and *whiI* under control of the constitutive *ermE** promotor. When *whiH* and *whiI* were overexpressed together in the *ΔwhiG* mutant, it caused a hypersporulation phenotype identical to the effect of overexpressing

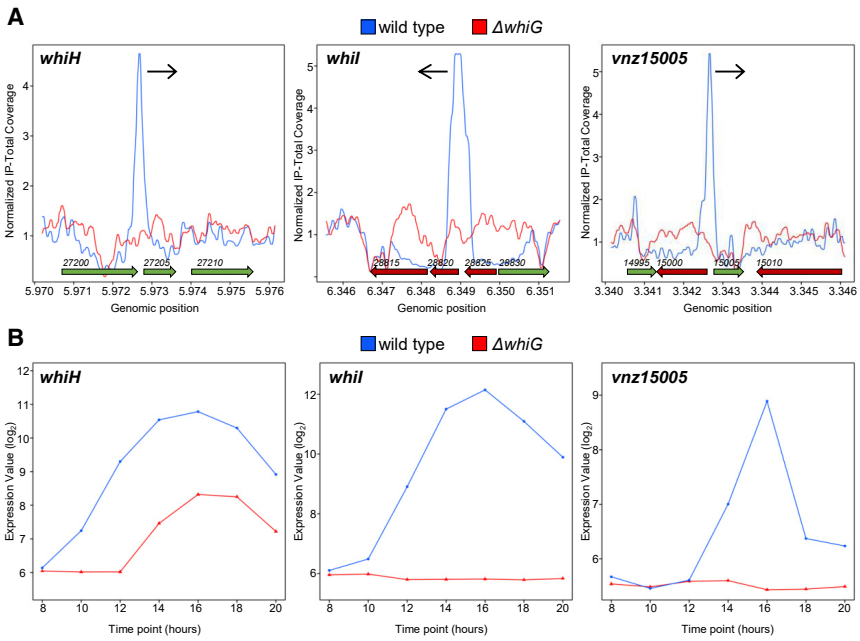

Figure 2. The σ^{WhiG} Regulon

(A) ChIP-seq data for the three σ^{WhiG} target genes *whiH*, *whiI*, and *vnz15005*. The plots span approximately 3 kb of DNA sequence. Genes running from right to left are shown in red, and genes running from left to right are shown in green. The black arrow indicates the genes transcribed by $E\sigma^{WhiG}$.

(B) Transcriptional expression profiles of *whiH*, *whiI*, and *vnz15005* in WT *S. venezuelae* and in the congenic *whiG* null mutant during submerged sporulation. In each panel, the x axis indicates the age of the culture in hours, and the y axis indicates the normalized transcript abundance (log_2).

(C) Sequence alignment of σ^{WhiG} target promoters and comparison with the consensus sequence for true flagellar σ factors (Helmann, 1991). Transcription start sites (TSSs), shown in green, were determined as part of a genome-wide TSS mapping experiment. Putative −10 and −35 sequences are shown in red. Note that the spacing between the putative -10 and -35 sequences of the σ^{WhiG} target promoters is N16, while it is N15 for true flagellar σ factors.

whiG in WT *S. venezuelae* (Figure 3). This experiment provides strong evidence that the main function of σ^{WhiG} is to direct transcription of just two targets, the genes encoding the key late developmental regulators WhiI and WhiH. WhiI is an orphan response regulator that is essential for the late stages of sporulation, when it forms a functional heterodimer with a second orphan response regulator, BldM, enabling WhiI to bind to DNA and regulate the expression of ~40 sporulation genes (Al-Bassam et al., 2014). WhiH is a GntR-family transcriptional regulator that also controls a large regulon of late sporulation genes (unpublished data). Thus, σ^{WhiG} indirectly activates expression of more than 100 late sporulation genes via WhiH and WhiI.

σ^{WhiG} Activity Is Not Correlated with σ^{WhiG} Protein Levels

To compare σ^{WhiG} protein levels and σ^{WhiG} activity during differentiation, we made protein and RNA extracts from the same WT developmental time course. Western blotting revealed that σ^{WhiG} was present at all developmental phases, with levels remaining constant to 15 h post-inoculation and only increasing about 2-fold across the life cycle (Figures 4A and 4B). In contrast, *whiI* mRNA levels, used as a proxy for σ^{WhiG} activity, increased almost 15-fold between 10 and 15 h (Figure 4C). The disparity between σ^{WhiG} protein levels and *whiI* transcript levels suggested that σ^{WhiG} might be subject to post-translational control that prevents activation of its target promoters at certain times during development.

A likely means for the post-translational control of a σ factor would be sequestration from RNA polymerase (RNAP) by an anti-σ factor. Anti-σ factors are typically encoded next to their cognate σ factors, but no proteins homologous to known anti-σ factors are encoded within 50 kb of *whiG*. Although it has diverged functionally, σ^{WhiG} belongs to the flagellar clade of σ factors, and in motile bacteria, the flagellar σ is inhibited by the anti-σ factor FlgM (Hughes et al., 1993; Hughes and Mathee, 1998; Helmann, 1999; Sorenson et al., 2004; Hsueh et al., 2011; Calvo and Kearns, 2015). However, no FlgM homolog is encoded in the *S. venezuelae* genome. Thus, for these reasons, we were unable to identify a candidate σ^{WhiG} anti-σ factor by bioinformatic means.

RsiG Is a σ^{WhiG} Cognate Anti-σ Factor Regulating the Progression of Multicellular Differentiation

To search for a candidate anti-σ factor, we screened a bacterial adenylate cyclase two-hybrid (BACTH) shotgun *S. venezuelae* genomic library using *whiG* as bait. Of 30 sequenced positive clones, ten were found to carry in-frame fusions to the same gene, *vnz19430*. Subsequently, we tested full-length Vnz19430 against full-length σ^{WhiG} in the BACTH system and found strong interaction (Figure 4E). *vnz19430* encodes a soluble, 24-kDa protein of previously unknown biochemical function. This gene was originally identified as a locus affecting morphological differentiation in the streptomycin producer *Streptomyces griseus* (Kudo et al., 1995; Yonekawa et al., 1999), where it was named *amfC*, but no specific role in development was established. Based on the work described below, we renamed this gene *rsiG* (regulator

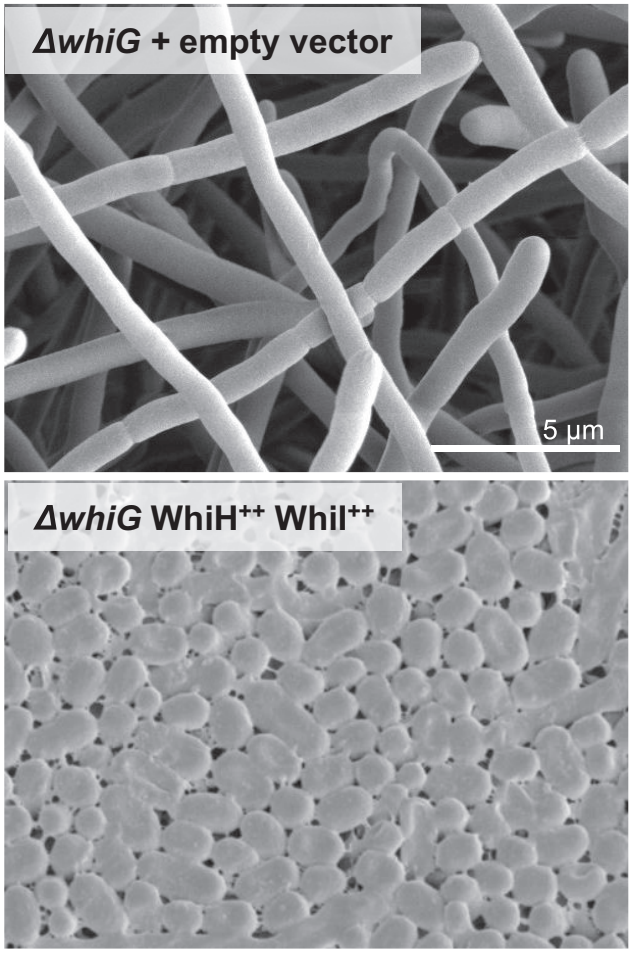

Figure 3. Overexpression of *whiH* and *whiI* Together Recapitulates the *whiG* Overexpression Phenotype

Scanning electron micrographs of the *whiG* mutant carrying the empty vector and the *whiG* mutant overexpressing *whiH* + *whiI*. Strains were imaged after 4 days of growth on MYM medium.

of sigma WhiG). RsiG is unrelated to any previously identified anti-σ factor and is encoded ~1.5 Mbp away from the *whiG* gene on the *S. venezuelae* chromosome.

To assess whether RsiG and σ^{WhiG} form a direct complex, we co-overexpressed the two proteins in *E. coli*, with σ^{WhiG} carrying an N-terminal His tag. When *S. venezuelae* σ^{WhiG} was expressed by itself, much of the protein was found in inclusion bodies. However, when RsiG and σ^{WhiG} were coexpressed, σ^{WhiG} was soluble. Further, RsiG co-purified with His-tagged σ^{WhiG} on a nickel column in approximately stoichiometric amounts, showing that RsiG and σ^{WhiG} form a direct complex (Figure 4F).

To confirm that RsiG regulates σ^{WhiG} activity *in vivo*, we next examined the phenotype associated with *rsiG* deletion. In striking similarity to the σ^{WhiG} overexpression phenotype, deletion of *ΔrsiG* caused a hypersporulation phenotype in which the vegetative hyphae differentiated into spore chains, again resulting in mature colonies with a biomass that consisted almost entirely of spores (Figure 4G). Because *S. venezuelae* can complete its life cycle in liquid culture (Schlimpert et al., 2016, 2017), we also examined developmental phenotypes in a microfluidic device using time-lapse fluorescence microscopy. Strains expressing an FtsZ-YPet fusion were introduced into the microfluidic system, and images were taken every 20 min to track development. In WT *S. venezuelae*, there was a period of vegetative growth during which the appearance of sporadic vegetative cross-walls could be seen. This was followed by a sporulation phase, in which less than half of the hyphae formed spore chains (Figure S1; Video S1). In contrast, when σ^{WhiG} was overexpressed, we observed a period of vegetative growth of similar length as that seen in the WT, but the subsequent sporulation phase was associated with a much more dramatic increase in the FtsZ-YPet signal, and the entire hyphal biomass was seen to sporulate (Figure S1; Video S2). The *ΔrsiG* mutant showed a similar phenotype as the σ^{WhiG} overexpression strain, but hypersporulation was less dramatic (Figure S1; Video S3).

Next we examined *whiI* mRNA levels, used as a proxy for σ^{WhiG} activity, in a developmental time course of the *rsiG* null mutant. Deletion of *rsiG* causes a dramatic increase in *whiI* transcription (Figure 4D). Thus, the hypersporulation phenotype of the *rsiG* mutant correlates with greatly increased expression of a σ^{WhiG} target gene. Each of the above phenotypes is consistent with RsiG acting as a σ^{WhiG}-specific anti-σ *in vivo*.

Crystal Structures Reveal c-di-GMP-Mediated RsiG-σ^{WhiG} Complex Formation

Because RsiG shows no homology to any known anti-σ factor, it was unclear how it might bind and affect the function of σ^{WhiG}. Thus, to address this question, we determined crystal structures of the complex. Two crystal forms were obtained (Table S1). The structure of crystal form 1 was solved by selenomethionine single-wavelength anomalous diffraction (SAD) and refined to R_{work}/R_{free} values of 19.5%/23.8% to 2.08-Å resolution (Figure 5A). This structure was then used to determine the structure of crystal form 2, which was refined to final R_{work}/R_{free} values of 20.9%/27.9% to 3.00-Å resolution. Both structures reveal a 1:1 RsiG:σ^{WhiG} complex, with crystal form 1 having one RsiG-σ^{WhiG} complex in the crystallographic asymmetric unit (ASU) and crystal form 2 having three complexes in the ASU. The four complex structures are essentially identical and can be superimposed with root-mean-square deviations (RMSDs) of 0.64–0.75 Å for the corresponding Cα atoms of the complex (Figure S2). Strikingly, each RsiG-σ^{WhiG} structure revealed the presence of a c-di-GMP dimer located at the σ^{WhiG}-RsiG interface (Figures 5A and 5B; Video S4). The c-di-GMP molecules appear to be key for complex formation by linking the proteins. Because no c-di-GMP was added prior to crystallization, the c-di-GMP molecules must have copurified with the complex from the *E. coli* expression system.

In the structure of the RsiG-σ^{WhiG} complex, σ^{WhiG} adopts a compact form (Figure 5A). σ^{WhiG} is a type 3 σ factor and, thus, contains three σ domains: σ_2 (residues 24–120, green in Figure 5A), σ_3 (residues 121–171, brown), a linker that connects σ_3 to σ_4 (residues 172–183, wheat), and σ_4 (residues 216–275, pale green). σ^{WhiG} also harbors an extra N-terminal helix, α1, preceding the σ_2 domain, which provides contacts to RsiG (Figure 5A). Structural homology (Dali) searches reveal that, as

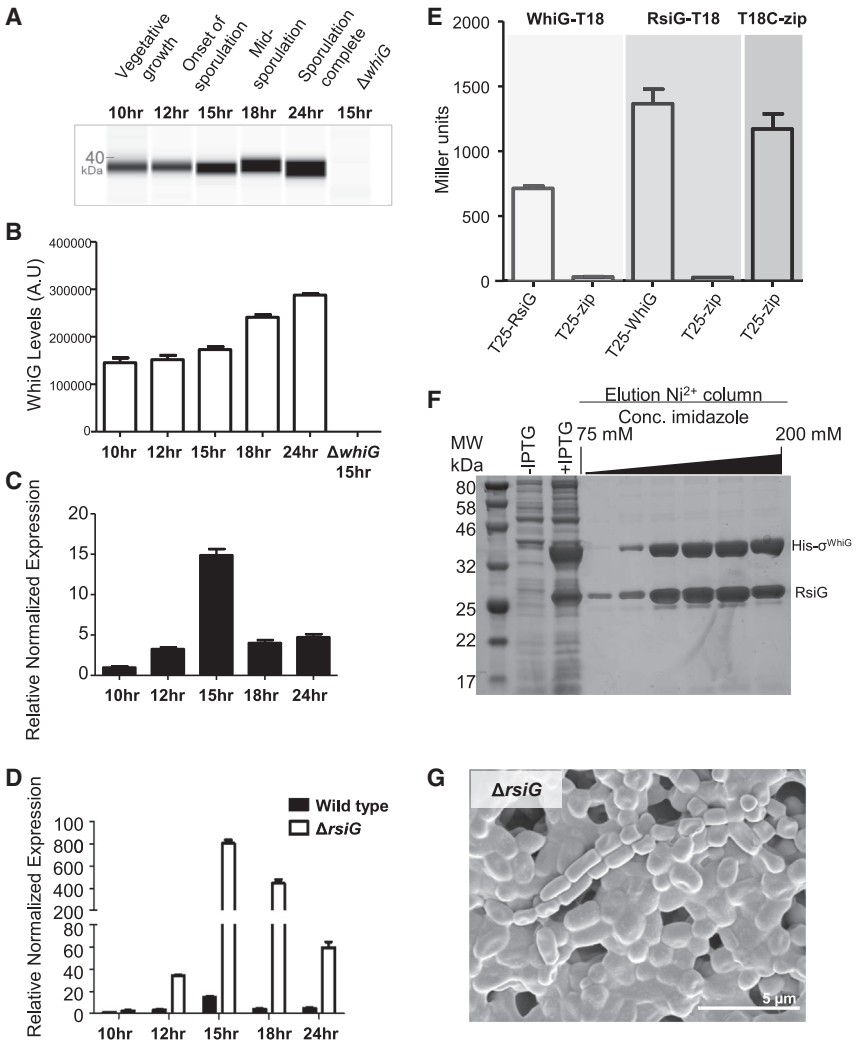

Figure 4. σ^{WhiG} Activity Is Regulated Post-translationally by a Novel Anti-σ, RsiG

(A) Automated western blot analysis showing σ^{WhiG} protein levels throughout development in Difco Nutrient Broth (DNB) medium, generated using the quantitative Wes capillary electrophoresis and blotting system (ProteinSimple, San Jose, CA; STAR Methods). Equal amounts (2.5 μg) of total protein were loaded for each sample, and σ^{WhiG} was detected with a polyclonal anti-σ^{WhiG} antibody. A single replicate is shown for each strain.

(B) Quantification of σ^{WhiG} levels (area under each peak, a.u.). All samples were analyzed in triplicate, and the mean value and its SE are shown for each sample.

(C) *whiI* mRNA abundance in the WT during submerged sporulation, determined by qRT-PCR. Expression values are calculated relative to the *hrdB* reference, normalized to the value at 10 h. RNA samples were prepared from the same culture as the protein samples analyzed in (A) and (B). All samples were analyzed in triplicate, and the mean value and its SE are shown for each sample.

(D) *whiI* mRNA abundance during submerged sporulation in the *rsiG* mutant, determined by qRT-PCR. Expression values are calculated relative to the *hrdB* reference, normalized to the WT value at 10 h. The data for the WT are replotted from (C). All samples were analyzed in triplicate, and the mean value and its SE are shown for each sample.

(E) Bacterial two-hybrid analysis to investigate the interaction between σ^{WhiG} and RsiG. The listed pairs of constructs were transferred into the BACTH reporter strain *E. coli* BTH101 by transformation. The resulting transformants were selected on L Broth agar containing 100 μg/mL carbenicillin and 50 μg/mL kanamycin and incubated at 37°C before single colonies were picked and subjected to β-galactosidase assays. Strains expressing fusions of both adenylate cyclase domains to the leucine zipper domain of GCN4 (zip) served as a positive control, whereas strains expressing fusions of one adenylate cyclase domain to a zip domain and the other to either WhiG or RsiG served as negative controls. Results are the average of three replicate cultures derived from the same single colony. Error bars represent SEM.

(F) Co-expression and purification of a soluble σ^{WhiG}-RsiG complex. σ^{WhiG} and RsiG were co-overexpressed in *E. coli* using pCOLADuet-1, with σ^{WhiG} carrying an N-terminal His tag. Following co-overexpression, the soluble extract was passed over a nickel column, and, after washing, bound proteins were eluted and analyzed on a 12% SDS-polyacrylamide gel.

(G) Deletion of *rsiG* leads to hypersporulation on solid medium. Shown is a scanning electron micrograph of the *rsiG* mutant imaged after 7 days of growth on Difco Nutrient Agar (DNA) medium.

See also Figure S1 and Video S3 for the effect of deleting *rsiG* on sporulation in liquid culture.

expected, each domain of σ^{WhiG} is structurally similar to the corresponding domains of other σ factors. Like other σ_2 domains, the σ^{WhiG} σ_2 domain core consists of three α helices (α2–α4), and the σ^{WhiG} σ_4 domain consists of four α helices (α9–α12). Residues 184–215, which comprise part of the σ_3-σ_4 linker, are disordered in the σ^{WhiG} structures. Individual σ regions are flexibly linked and adopt multiple orientations when not in complex with RNAP or an anti-σ factor (Feklístov et al., 2014). Thus, it was interesting that Dali searches revealed that σ^{WhiG} domains σ_2 and σ_4 superimpose well as a unit onto the same regions of the σ^{28} structure that was solved bound to its anti-σ factor, FlgM, despite their σ_3 domains adopting distinct orientations (Sorenson et al., 2004; Figure S3A). In the σ^{FliA}-FlgM complex, the σ_3 region of σ^{FliA} has an elongated α3, and its compact structure is stabilized by a salt bridge between Glu145, located on α3 of σ_3, and Arg115 from its σ_2 domain. The conservation of these residues, combined with crosslinking data, led to the suggestion that this salt bridge may form in all related σ factors and stabilize the apo form (Sorenson et al., 2004; Sorenson and Darst, 2006). Notably, these residues and the corresponding salt bridge are indeed conserved in σ^{WhiG}, even though, as noted, the σ^{WhiG} σ_3 domain does not have an elongated α3. In σ^{WhiG}, the corresponding salt bridge is formed between Glu180 on α4 helix of σ_3 and the conserved Arg82 on σ_2 (Figure S3A). These findings

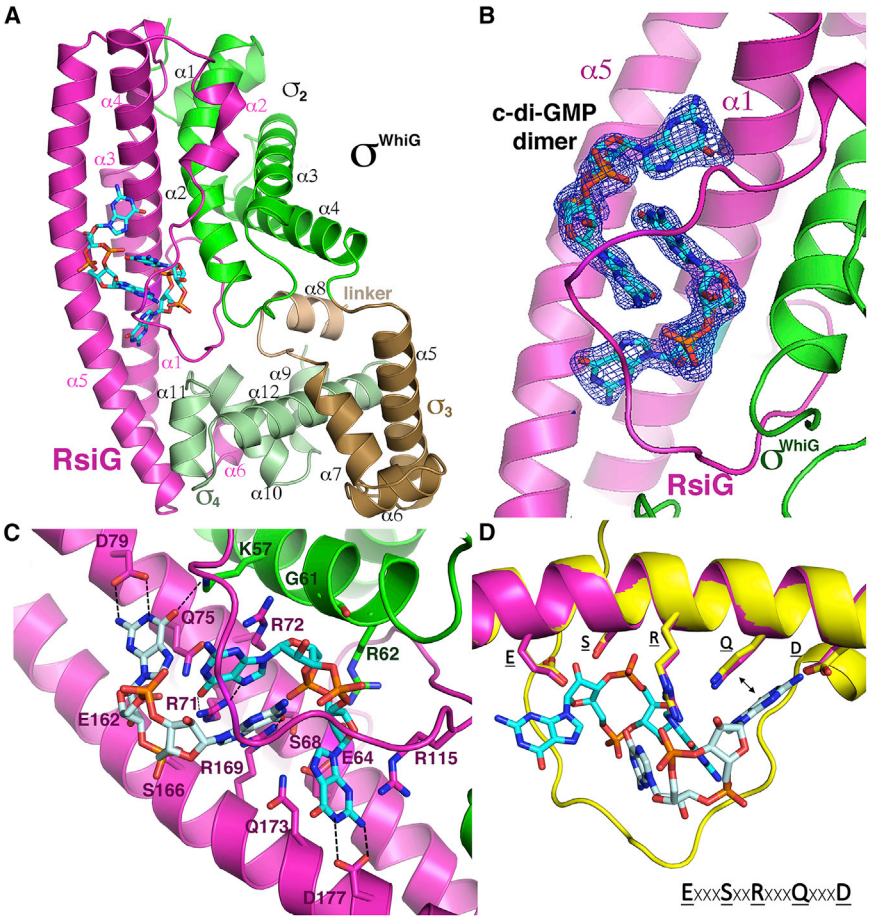

Figure 5. Structure of the *S. venezuelae* RsiG-σ^{WhiG} Complex

(A) Ribbon diagram of the overall structure of the RsiG-σ^{WhiG} complex. RsiG is colored magenta. The σ regions of σ^{WhiG} are colored green, brown, and pale green for the σ_2, σ_3 and σ_4 domains, respectively. The linker between σ_3 and σ_4 is colored wheat. The c-di-GMP dimer is shown as sticks. RsiG, σ^{WhiG}, their secondary structural elements, and the σ regions of σ^{WhiG} are labeled.

(B) Close-up of the c-di-GMP partially intercalated dimer with a Fo-Fc omit map included. The Fo-Fc map is shown as a blue mesh and contoured at 3.5 σ.

(C) Selected c-di-GMP interactions with RsiG and σ^{WhiG}. Note the two-fold symmetry evident in the interactions between the c-di-GMP dimer and the $E(X)_3S(X)_2R(X)_3Q(X)_3D$ repeat motif found on each coiled-coil helix.

(D) Superimposition of RsiG coiled coils. One $E(X)_3S(X)_2R(X)_3Q(X)_3D$ repeat motif (magenta) was overlaid onto the second repeat (yellow). The result is that the motif residues that contact the c-di-GMP molecules also superimpose identically. The consensus repeat motif, ExxxSxxRxxxQxxxD, is included below the structure superimposition.

See also Figure S2 for superimposition of the two solved RsiG-σ^{WhiG} structures as well as Figure S3 for detailed interactions within the complex.

suggest that this interaction can be maintained in different structural contexts for related type 3 σ factors.

The majority of the contacts from the anti-σ factors FlgM (Sorenson et al., 2004) and RsiG are to the σ_2 and σ_4 domains of their σ partner. However, the similar relative conformations of the σ_2 and σ_4 domains in σ^{WhiG} and σ^{28} do not reflect similar interactions with their anti-σ factors. RsiG makes distinct contacts with σ^{WhiG} and also has a fold that is entirely different from FlgM, consisting of 6 α helices. Indeed, the RsiG structure is distinct from any previously solved structure in the protein database; Dali searches failed to identify any structure similar to RsiG. A striking feature of the RsiG structure is the presence of an extended antiparallel coiled coil formed by helices α1 and α5 (Figure 5A). These two helices are connected to short helices (α2, α3, α4, and α6) that brace RsiG to the sides of σ^{WhiG}. Helix α2 is connected to α3-α4 by a long, meandering loop (residues 104–125) that encircles the bound c-di-GMP (Figure 5A).

The RsiG-σ^{WhiG} Interaction Is Mediated by a Unique c-di-GMP Dimer

σ^{WhiG} is a key regulator of the late stage of *Streptomyces* development, differentiation of the reproductive hyphae into spores. The finding that c-di-GMP mediates RsiG-σ^{WhiG} complex formation reveals c-di-GMP as the central integrator of *Streptomyces* development; we showed recently that the activity of the master repressor BldD, which controls the initial onset of *Streptomyces* development, is itself controlled by a c-di-GMP tetramer (Tschowri et al., 2014; Schumacher et al., 2017). In the RsiG-σ^{WhiG} structure, c-di-GMP promotes the correct conformation of RsiG for σ^{WhiG} binding and locks the proteins together. The c-di-GMP dimer bound in the RsiG-σ^{WhiG} complex is also different from c-di-GMP dimers found in previously solved structures of DNA regulatory proteins or other physiologically established c-di-GMP complexes. Specifically, in previous structures of c-di-GMP dimers bound to regulators, the four guanine bases make classical stacking interactions to form intercalated dimers (Krasteva et al., 2010; Matsuyama et al., 2016; Schumacher et al., 2016; Schumacher and Zeng, 2016; Wang et al., 2016; Raju and Sharma, 2017). In contrast, in the RsiG-σ^{WhiG}-bound c-di-GMP dimer, only the two central bases are stacked, whereas both guanine bases at the edges of the dimer are rotated out of the stacking plane, placing them nearly perpendicular to the central bases (Figures 5B and 5C). Further, the c-di-GMP-bound dimer adopts a symmetrical structure because of the equivalence of contacts from the conserved residues of the coiled-coil repeat elements. Indeed, although the two helices of the coiled coil are not formed by dimerization of two separate subunits, each of the coiled-coil helices has an $E(X)_3S(X)_2R(X)_3Q(X)_3D$ repeat (RsiG residues 64–79 [repeat 1] and residues 162–177 [repeat 2]), where the conserved E, S, R, Q, and D from each motif make identical contacts to the

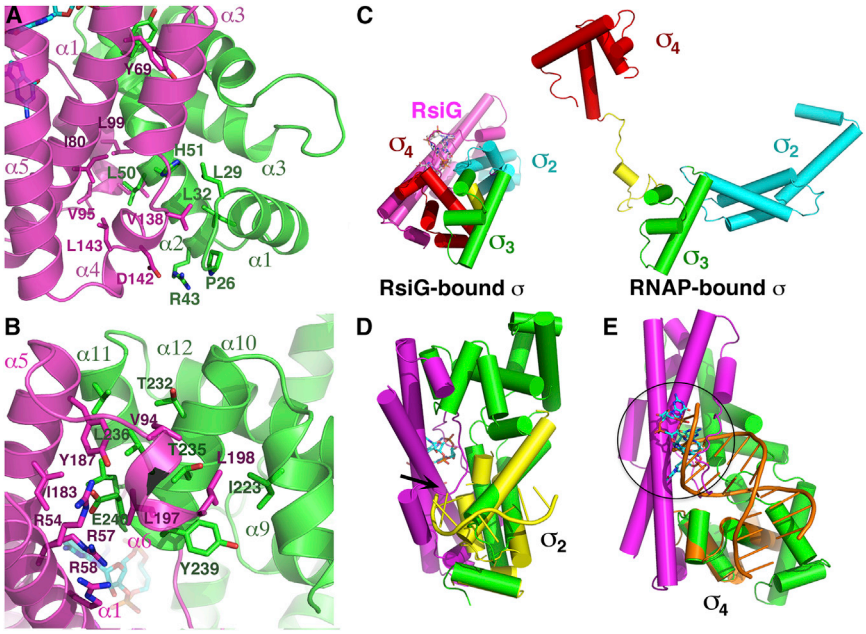

Figure 6. RsiG-σ^{WhiG} Complex Interactions and the Mechanism of σ^{WhiG} Inhibition by RsiG

(A) Close-up of the interaction interface between RsiG (colored magenta) and the σ_2 domain of σ^{WhiG} (colored green). Residues that make contacts are shown as sticks and are labeled.

(B) Interaction interface of RsiG (colored magenta) and the σ_4 domain of σ^{WhiG}. As in (A), residues that make contacts are shown as sticks and are labeled.

(C) Comparison of the structures of RsiG-bound σ^{WhiG} (left) and RNAP-bound σ (right). The σ_3 regions of each σ factor (both colored green) are shown in the same orientation to allow direct comparison. The σ_2 and σ_4 domains are colored cyan and red, respectively, and RsiG is colored magenta. Note that the RsiG-bound σ^{WhiG} is compact in shape, in contrast to the extended RNAP-bound σ.

(D) Overlay of the σ_2 region of RsiG-bound σ^{WhiG} with the *E. coli* σ^{E}_2 bound to the −10 DNA element, showing that the DNA would clash with RsiG in the RsiG-σ^{WhiG} complex.

(E) Overlay of the σ_4 region of RsiG-bound σ^{WhiG} with the *E. coli* σ^{E}_4 complexed to the −35 DNA element. Here, the DNA would clash with the c-di-GMP molecules bound to the RsiG-σ^{WhiG} complex (circled).

c-di-GMP molecules (Figure 5D; Video S4). Remarkably, when repeat 1 from a RsiG-σ^{WhiG} complex is overlaid onto repeat 2, the other repeat elements also become overlaid, as do the c-di-GMP dimers (Figure S3B; Figure 5D). Thus, the repeat motif is located in the same position on each helix of the coiled coil, which suggests that the helices may have arisen from an intragenic duplication event (see Discussion).

In the RsiG-σ^{WhiG} complex, each conserved residue of the $E(X)_3S(X)_2R(X)_3Q(X)_3D$ repeat motif contacts a c-di-GMP molecule. The serines of the motif help position the conserved glutamic acid and arginine side chains to interact with the c-di-GMP molecules while also contacting the c-di-GMP phosphates. The glutamic acid side chains of residues Glu64 and Glu162 interact with ribose hydroxyl groups. The $Q(X)_3D$ motif is responsible for recognizing the rotated guanine bases at each end of the c-di-GMP dimer, and the aspartic acids Asp79 and Asp177 recognize the Watson Crick faces of these guanines, and the glutamines Gln75 and Gln173 stack against the rotated bases (Figure 5C; Figure S3C). The conserved arginines from each motif, Arg71 and Arg169, read the stacked guanines located at the center of the c-di-GMP dimer by hydrogen bonding to the O6 and N7 atoms of the bases (the Hoogsteen face). Thus, the contacts from the conserved aspartic acids and arginines provide base specificity. The contacts from the RsiG coiled-coil helices also anchor the c-di-GMP dimer in place, positioning it to make interactions with multiple RsiG loop residues. Specifically, Asp106 and His110 make phosphate backbone contacts to c-di-GMP, His110 and Arg115 provide stacking interactions via their side chains, Ser108 contacts a guanine base, and Ser112 interacts with a c-di-GMP phosphate group (Figure S3C). These interactions from the c-di-GMP dimer to the middle of the RsiG loop help anchor it against σ^{WhiG}. Although most of the interactions with c-di-GMP in the complex are mediated by RsiG, σ^{WhiG} residues Lys57, Gly61, and Arg62 from α helix 2 of the σ^{WhiG} σ_2 domain also interact with the c-di-GMP dimer (Figure 5C). σ^{WhiG} residue Gly61, which packs against one of the ribose groups of c-di-GMP, plays an important role in this interaction because of its small size; any side chain at this position of σ^{WhiG} would clash with the c-di-GMP. Notably, multiple sequence alignments show that the residues from RsiG and σ^{WhiG} that contact c-di-GMP are highly conserved among protein homologs, in particular the key c-di-GMP binding residues from the $E(X)_3S(X)_2R(X)_3Q(X)_3D$ repeat motifs (see Discussion).

RsiG-c-di-GMP Interaction with σ^{WhiG} and Inhibition of σ^{WhiG} Sigma Function

The bound c-di-GMP dimer ties RsiG and σ^{WhiG} together by mediating contacts to each protein and also by acting as a chaperone to enable folding of the RsiG loop around σ^{WhiG}. This interaction results in burial of a sizeable 2,353 $Å^2$ of the RsiG and σ^{WhiG} surface from solvent. The N-terminal helix and helices α2 and α3 of the σ^{WhiG} σ_2 domain make extensive contacts to RsiG helices α2, α3, and α4. The C-terminal portion of the first helix of the RsiG coiled coil (residues 69–80) also contributes to this σ^{WhiG} binding surface. This contact region is primarily hydrophobic, with σ^{WhiG} residue Leu50 inserting into a RsiG hydrophobic pocket composed of residues Ile80, Val95, Leu99, and Leu143 and RsiG residue Val138 interfacing with σ^{WhiG} residues Pro26, Leu29, Leu32, and His51 (Figure 6A). In addition, there are stacking interactions between RsiG Tyr69 and σ^{WhiG} Tyr58 and a salt bridge between RsiG Asp142 and σ^{WhiG} Arg43 (Figure 6A). The RsiG loop that folds around the c-di-GMP molecules fills a gap between the σ_2 and σ_4 domains in the otherwise compact σ^{WhiG} structure, which helps brace σ_4 against RsiG (Figure 5A). This loop region is also the only contact from RsiG to σ^{WhiG} σ_3. Although the RsiG loop stabilizes σ_4 in position, residues from

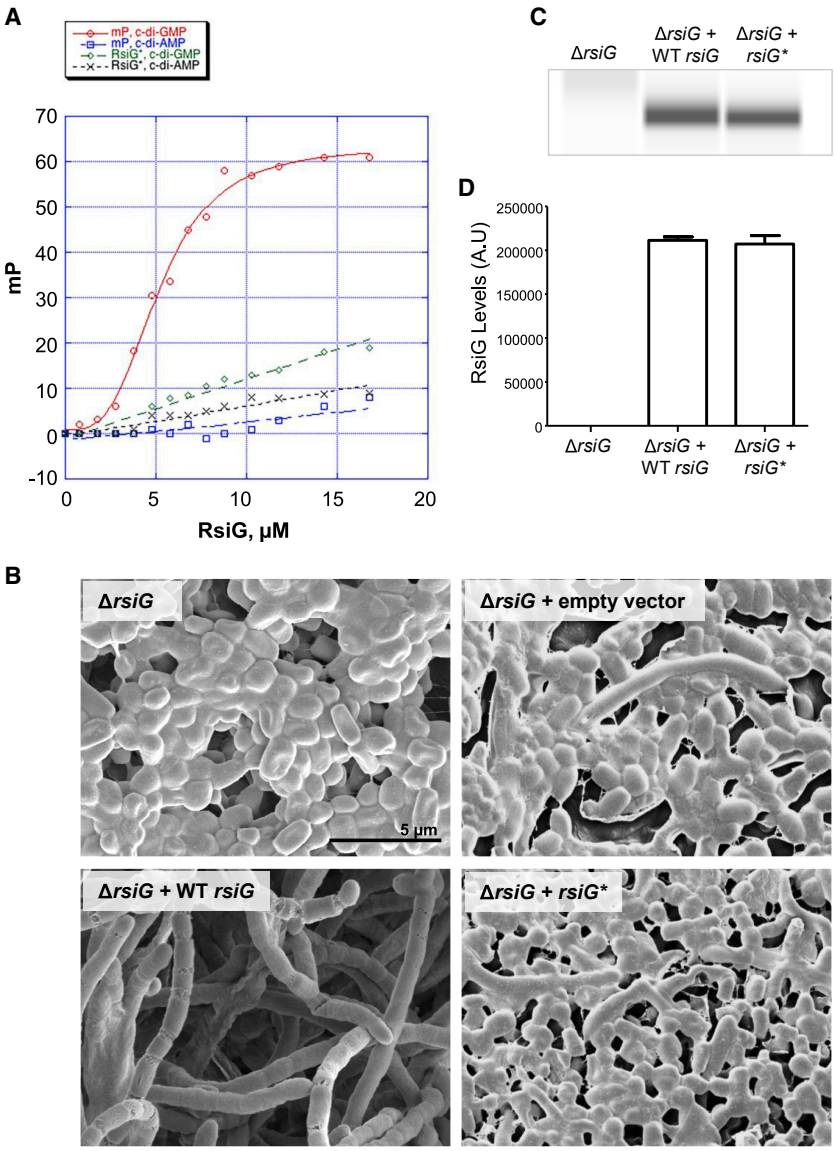

Figure 7. Creation of an RsiG Derivative Defective in c-di-GMP Binding (RsiG*) and Demonstration that c-di-GMP Binding Is Required for RsiG Activity *In Vivo*

(A) Fluorescence polarization (FP)-based binding isotherms of WT RsiG binding to 2′-Fluo-AHC-c-di-GMP (red circles), WT RsiG binding to 2′-Fluo-AHC-c-di-AMP (blue squares), RsiG* binding to 2′-Fluo-AHC-c-di-GMP (green diamonds), and RsiG* binding to 2′-Fluo-AHC-c-di-AMP (black crosses). Each binding curve is a representative from 3 technical replicates. The y axis shows millipolarization units (mP), and the x axis shows the concentration of RsiG protein (micromolar).

(B) Scanning electron micrographs showing that deletion of *rsiG* causes hypersporulation and that the *rsiG* mutant can be complemented with WT *rsiG* but that it cannot be complemented with the *rsiG** allele (R71A, D79A, R169A, D177A) encoding a protein defective in c-di-GMP binding. Strains were imaged after 7 days of growth on DNA medium.

(C) RsiG* is not affected regarding protein stability. Shown is an automated western blot analysis comparing RsiG protein levels in the *rsiG* mutant complemented with the WT *rsiG* allele and the *rsiG** allele, generated using the quantitative Wes capillary electrophoresis and blotting system (ProteinSimple, San Jose, CA; STAR Methods). Equal amounts (2.5 μg) of total protein were loaded for each sample, and RsiG was detected with a polyclonal anti-RsiG antibody. A single replicate is shown for each strain. Strains were grown in DNB, and samples were collected at 15 h.

(D) Quantification of RsiG levels (area under each peak, a.u.).

All samples were analyzed in triplicate, and the mean value and its SE are shown for each sample. See also Figure S4 for biochemical analysis of the dependence of complex formation on c-di-GMP as well as Figure S5 for conservation of c-di-GMP-binding residues among homologs of RsiG and σ^{WhiG}.

the N-terminal and C-terminal ends of the RsiG coiled coil and the last RsiG helix, α6, present an extensive surface for contacting σ_4 helices α9–α11. This interaction is also largely hydrophobic, with σ^{WhiG} residues Ile223, Thr232, Thr235, Leu236, Tyr239, and Leu242 interacting with RsiG residues Ile183, Tyr187, Leu197, and Leu198. Hydrogen bond or electrostatic interactions are also found between σ^{WhiG} residue Glu240 and RsiG residues Arg54, Arg57, Arg58, and Tyr187 (Figure 6B).

σ factors play a key role in bacterial transcription, associating with RNAP to dictate the promoter specificity of the resulting holoenzyme. Promoter specificity is determined principally by the σ_2 and σ_4 domains, which bind to the −10 and −35 regions of the promoter, respectively (Feklístov et al., 2014). When σ factors bind RNAP, they form a highly extended structure that is exposed for promoter contact (Figure 6C). Most of the structures available for anti-σ-σ complexes have been determined for the smaller extracytoplasmic function (ECF) or group IV σ factors, which contain only domains σ_2 and σ_4 (Hughes and Mathee, 1998; Campagne et al., 2015; Paget, 2015). Structures of σ factors bound to ECF anti-σ factors have revealed that most of these anti-σ factors contact both the σ_2 and σ_4 regions (Campagne et al., 2015; Schumacher et al., 2018), whereas structures of anti-σ factors complexed with larger σ factors often only contact one σ factor domain (Campbell et al., 2002; Lambert et al., 2004; Patikoglou et al., 2007; Wei et al., 2019). Indeed, aside from the RsiG-σ^{WhiG} complex, the only other non-ECF anti-σ-σ complex revealing binding of multiple σ domains by the anti-σ is the *Aquifex aeolicus* FliA-FlgM complex (Sorenson et al., 2004). Analysis of the RsiG-σ^{WhiG} structure reveals that RsiG binding inactivates the sigma function of σ^{WhiG} in multiple ways. First, when bound to RsiG, σ^{WhiG} adopts a highly compact structure where the σ_2 and σ_4 domains are separated by ~25 Å

(measured from center to center) compared with ~70 Å when bound to RNAP (Figure 6C). Second, superimposition of σ_2 and σ_4 of σ^{WhiG} onto *E. coli* $\sigma^{E}{}_2$ bound to its −10 element and *E. coli* $\sigma^{E}{}_4$ bound to its −35 element, respectively, reveals multiple points of clash with the promoter DNA (Figures 6D and 6E). Thus, these analyses show that the RsiG-bound σ^{WhiG} would be unable to form an active holoenzyme with RNAP.

c-di-GMP Controls RsiG-σ^{WhiG} Complex Formation

The structure of the RsiG-(c-di-GMP)$_2$-σ^{WhiG} complex suggested that RsiG would likely be able bind c-di-GMP in the absence of σ^{WhiG}. To test this hypothesis and to quantify any interaction, we performed fluorescence polarization (FP)-based binding experiments. These studies were carried out with the fluoresceinated probe 2′-Fluo-AHC-c-di-GMP. This probe harbors a fluorescein dye on one ribose, which, our structures revealed, would not block binding to RsiG. The FP experiments showed that RsiG alone binds 2′-Fluo-AHC-c-di-GMP with a K_d of 6.5 ± 1.5 μM (Figure 7A). RsiG showed no binding to the identically fluoresceinated c-di-AMP derivative 2′-Fluo-AHC-c-di-AMP (Figure 7A). We next examined binding of c-di-GMP to RsiG-σ^{WhiG}. These analyses resulted in a K_d of 0.39 ± 0.05 μM (Figure S4A), indicating that the complex binds c-di-GMP with much higher affinity than RsiG alone. This is consistent with the finding that, although RsiG provides most of the contacts to c-di-GMP, σ^{WhiG} also contacts c-di-GMP, but, more importantly, σ^{WhiG} appears to aid in folding or stabilizing the correct conformation of RsiG required for c-di-GMP binding.

The ability of RsiG to discriminate between c-di-GMP and c-di-AMP was consistent with the crystal structure, which showed that the arginine and aspartic acid residues in the two $E(X)_3S(X)_2R(X)_3Q(X)_3D$ motifs make base-specifying contacts to the guanines of the c-di-GMP dimer. To disrupt c-di-GMP binding by RsiG, we substituted the arginine and aspartic acid residues in both $E(X)_3S(X)_2R(X)_3Q(X)_3D$ motifs with alanines to create RsiG* (R71A, D79A, R169A, D177A). RsiG* failed to bind 2′-Fluo-AHC-c-di-GMP in FP assays and also, as expected, did not bind 2′-Fluo-AHC-c-di-AMP (Figure 7A). Overall, these data demonstrate unequivocally that anti-σ alone binds specifically to c-di-GMP but not to c-di-AMP and that the base-specifying arginine and aspartic acid residues of the $E(X)_3S(X)_2R(X)_3Q(X)_3D$ motif are essential for this interaction.

To determine whether c-di-GMP binding to RsiG is required for the anti-σ to sequester σ^{WhiG}, we coexpressed σ^{WhiG} and His_6-RsiG*. Although σ^{WhiG} copurified with WT His_6-RsiG, σ^{WhiG} did not copurify with His_6-RsiG* (Figure S4B). Further, we built a complementation construct expressing a protein solely defective in c-di-GMP binding (RsiG*) and found that it had no ability to complement an *S. venezuelae rsiG* mutant, in contrast to an otherwise identical construct expressing WT RsiG, which restored normal development (Figures 7B–7D). These data show that c-di-GMP mediates the ability of RsiG to restrain σ^{WhiG} activity *in vitro* and *in vivo*.

DISCUSSION

This work is the first to describe that c-di-GMP targets a σ factor and its functionality. As a result of this discovery, it is now clear that c-di-GMP signals through BldD and σ^{WhiG}, respectively, to control the two most dramatic transitions of the *Streptomyces* life cycle: the formation of reproductive aerial hyphae and their differentiation into spore chains. In both cases, c-di-GMP functions as a "brake." In the first case, BldD sits at the top of the developmental regulatory network, serving to repress a large set of genes, including many genes of the core transcriptional regulatory cascade itself. The ability of BldD to repress this suite of sporulation genes is dependent on binding to a tetrameric cage of c-di-GMP that acts as an inter-subunit linker, enabling BldD to dimerize and, hence, bind DNA (Tschowri et al., 2014; Schumacher et al., 2017; Bush et al., 2015). Thus, by signaling through the BldD$_2$-(c-di-GMP)$_4$ complex, c-di-GMP functions to prolong vegetative growth and prevent initiation of development. σ^{WhiG} acts later in the development pathway, after the formation of aerial hyphae, controlling the differentiation of these reproductive structures into spores. By driving σ^{WhiG} into an inactive RsiG-(c-di-GMP)$_2$-σ^{WhiG} complex, c-di-GMP acts to block this developmental transition. The difference between these two signaling events can be seen in the phenotypes associated with deletion of *bldD* or *rsiG* in *S. venezuelae*. When *rsiG* is deleted, the duration of vegetative growth seen in time-lapse imaging is the same as in the WT, but the subsequent sporulation phase is much more pronounced than in the WT (Figure S1; Videos S1 and S3). In contrast, deletion of *bldD* results in a short period of vegetative growth and precocious sporulation (Tschowri et al., 2014).

Global c-di-GMP levels fall sharply as *S. venezuelae* enters development (A. Latoscha and N. Tschowri, personal communication), and BldD dissociates from DNA before σ^{WhiG} is released from RsiG. The most parsimonious explanation for this order of events is the K_d values of the proteins for c-di-GMP. BldD binds 2′-Fluo-AHC-c-di-GMP with a K_d of 2.5 ± 0.6 μM (Tschowri et al., 2014), whereas the K_d for [RsiG + σ^{WhiG}] is 0.39 ± 0.05 μM, meaning that, as c-di-GMP levels drop, BldD would become inactive before σ^{WhiG} is released from RsiG. A more complex issue is how c-di-GMP levels are controlled. In *S. venezuelae*, there are 11 enzymes involved in c-di-GMP metabolism (Tschowri, 2016; Al-Bassam et al., 2018; Latoscha et al., 2019). Five of these are composite GGDEF-EAL proteins carrying both the synthetic and degradative domains, in most cases in combination with multiple regulatory domains (e.g., PAS GAF, PAC) that are likely to determine which activity is dominant, depending on regulatory inputs (Tschowri, 2016; Al-Bassam et al., 2018; Latoscha et al., 2019). Further, four of these genes (*cdgA*, *cdgB*, *cdgC*, and *cdgE)* are direct regulatory targets of BldD, creating numerous potential feedback loops (Tschowri, 2016; Al-Bassam et al., 2018; Latoscha et al., 2019). Thus, determining how *Streptomyces* controls c-di-GMP levels in time and space will be a major challenge in the future.

Like *whiG*, *rsiG* is present in more than 98% of the 802 complete and annotated *Streptomyces* genomes available at GenBank, suggesting that RsiG is likely to play a conserved function throughout the genus. In addition, RsiG can also be found outside of the Streptomycetes. In a search of 3,962 reference/representative bacterial genomes available at GenBank (60 of which are *Streptomyces* genomes), we found a total of 134 *rsiG* homologs, all exclusively in members of the phylum

Actinobacteria (Table S2). Outside of the genus *Streptomyces,* most *rsiG* homologs are found in members of the families Geodermatophilaceae and Pseudonocardiaceae.

All 134 genomes with an *rsiG* homolog also have a *whiG* homolog, suggesting that *whiG* always co-occurs with *rsiG*. Sequence logos derived from amino acid sequence alignments of RsiG and σ^{WhiG} homologs show that the residues that bind the cyclic dinucleotide in our structure are strikingly well conserved. Specifically, in RsiG, the two α helices involved in c-di-GMP binding both contain well-conserved $E(X)_3S(X)_2R(X)_3Q(X)_3D$ motifs (Figure S5A). The only exception occurs in the first of the two helices, where Gln75 in the *S. venezuelae* protein is frequently replaced with a histidine among RsiG homologs. Glutamine and histidine, however, are both highly suitable to make the stacking interaction with the guanine base of c-di-GMP seen in the *S. venezuelae* structure. The striking repetition of the $E(X)_3S(X)_2R(X)_3[Q/H](X)_3D$ motif in RsiG and the 33% overall sequence identity between the two α helices raises the possibility that they have arisen from an ancestral intragenic duplication event. The two residues of σ^{WhiG} that make direct contacts to c-di-GMP, Lys57 and Arg62, both of which are found in σ region 2.1, are also highly conserved among σ^{WhiG} homologs that co-occur with RsiG (Figure S5B). In addition, the glycine residue found at position 61 in *S. venezuelae* σ^{WhiG} is likely to be important for c-di-GMP binding because a larger side chain at that position would cause a steric clash. Consistent with this conclusion, Gly61 is not well conserved in the true flagellar σ factors from organisms that do not possess an *rsiG* homolog, such as *E. coli* σ^{28} and *B. subtilis* SigD (Sorenson et al., 2004), but this residue is highly conserved among the true σ^{WhiG} proteins that co-occur with RsiG (Figure S5B). The RsiG-σ^{WhiG} interface is complex and not as clearly defined as the residues required for c-di-GMP binding. However, many of the additional highly conserved residues we observed among σ^{WhiG} and RsiG homologs are involved in the interface between the two proteins (Figures S5A and S5B). Finally, all the Actinobacteria that encode a homolog of RsiG also encode DGCs, implying the presence of c-di-GMP. These combined observations suggest that this second messenger controls RsiG-σ^{WhiG} complex formation across the *Streptomyces* genus and beyond.

STAR★METHODS

Detailed methods are provided in the online version of this paper and include the following:

- KEY RESOURCES TABLE
- LEAD CONTACT AND MATERIALS AVAILABLITY
- EXPERIMENTAL MODEL AND SUBJECT DETAILS
- METHOD DETAILS
  - Bacterial strains, plasmids, media, and conjugations
  - Construction and complementation of S. venezuelae null mutants
  - Overexpression of proteins in S. venezuelae
  - Scanning Electron Microscopy
  - Chromatin immunoprecipitation, library construction, sequencing, and ChIP-seq data analysis
  - Microarray analysis
  - qRT-PCR
  - Western blotting
  - Bacterial two-hybrid genomic library construction, screening, and analysis
  - Overexpression and copurification of the σ^{WhiG} -RsiG complex
  - Crystallization and structure determination of the σ^{WhiG}-RsiG complex
  - Determination of the affinity and specificity of c-di-GMP for RsiG and RsiG-σ^{WhiG} by fluorescence polarization (FP)
  - Time-lapse imaging of S. venezuelae
- QUANTIFICATION AND STATISTICAL ANALYSIS
- DATA AND CODE AVAILABILITY

SUPPLEMENTAL INFORMATION

Supplemental Information can be found online at https://doi.org/10.1016/j.molcel.2019.11.006.

ACKNOWLEDGMENTS

We thank Jake Malone for comments on the manuscript, Félix Ramos-León for helpful discussions, Susan Schlimpert for assistance with time-lapse imaging and figures, Morgan Feeney for assistance with the Wes automated western blotting system, and BIO S&T (Saint-Laurent, Québec, Canada) for construction of the bacterial two-hybrid genomic libraries. This work was funded by BBSRC grant BB/N006852/1 (to M.J. Buttner), BBSRC Institute Strategic Programme grant BB/J004561/1 (to the John Innes Centre), and 1R35GM130290 (to M.A.S.).

AUTHOR CONTRIBUTIONS

K.A.G. and M.A.S. designed, performed, and interpreted experiments, made figures, and wrote the paper. M.J. Bush, M.J. Bibb, N.A.H., W.Z., M.H., H.Z., and K.C.F. designed and performed experiments. G.C. performed the bioinformatics analysis. R.G.B. interpreted results and wrote the paper. M.J. Buttner designed and interpreted experiments and wrote the paper.

DECLARATION OF INTERESTS

The authors declare no competing interests.

Received: September 3, 2019
Revised: October 22, 2019
Accepted: November 4, 2019
Published: December 3, 2019

SUPPORTING CITATIONS

The following references appear in the Supplemental Information: Crooks et al. (2004); Edgar (2004); Karimova et al. (1998).

REFERENCES

Adams, P.D., Afonine, P.V., Bunkóczi, G., Chen, V.B., Davis, I.W., Echols, N., Headd, J.J., Hung, L.W., Kapral, G.J., Grosse-Kunstleve, R.W., et al. (2010). PHENIX: a comprehensive Python-based system for macromolecular structure solution. Acta Crystallogr. D Biol. Crystallogr. *66*, 213–221.

Aínsa, J.A., Parry, H.D., and Chater, K.F. (1999). A response regulator-like protein that functions at an intermediate stage of sporulation in *Streptomyces coelicolor* A3(2). Mol. Microbiol. *34*, 607–619.

Al-Bassam, M.M., Bibb, M.J., Bush, M.J., Chandra, G., and Buttner, M.J. (2014). Response regulator heterodimer formation controls a key stage in *Streptomyces* development. PLoS Genet. *10*, e1004554.

Al-Bassam, M.M., Haist, J., Neumann, S.A., Lindenberg, S., and Tschowri, N. (2018). Expression patterns, genomic conservation and input into developmental regulation of the GGDEF/EAL/HD-GYP domain proteins in *Streptomyces*. Front. Microbiol. *9*, 2524.

Amikam, D., and Galperin, M.Y. (2006). PilZ domain is part of the bacterial c-di-GMP binding protein. Bioinformatics *22*, 3–6.

Baraquet, C., and Harwood, C.S. (2013). Cyclic diguanosine monophosphate represses bacterial flagella synthesis by interacting with the Walker A motif of the enhancer-binding protein FleQ. Proc. Natl. Acad. Sci. USA *110*, 18478–18483.

Bibb, M.J., Domonkos, A., Chandra, G., and Buttner, M.J. (2012). Expression of the chaplin and rodlin hydrophobic sheath proteins in *Streptomyces venezuelae* is controlled by σ^{BldN} and a cognate anti-sigma factor, RsbN. Mol. Microbiol. *84*, 1033–1049.

Boehm, A., Kaiser, M., Li, H., Spangler, C., Kasper, C.A., Ackermann, M., Kaever, V., Sourjik, V., Roth, V., and Jenal, U. (2010). Second messenger-mediated adjustment of bacterial swimming velocity. Cell *141*, 107–116.

Bush, M.J., Tschowri, N., Schlimpert, S., Flärdh, K., and Buttner, M.J. (2015). c-di-GMP signalling and the regulation of developmental transitions in streptomycetes. Nat. Rev. Microbiol. *13*, 749–760.

Bush, M.J., Chandra, G., Findlay, K.C., and Buttner, M.J. (2017). Multi-layered inhibition of *Streptomyces* development: BldO is a dedicated repressor of *whiB*. Mol. Microbiol. *104*, 700–711.

Calvo, R.A., and Kearns, D.B. (2015). FlgM is secreted by the flagellar export apparatus in *Bacillus subtilis*. J. Bacteriol. *197*, 81–91.

Campagne, S., Allain, F.H., and Vorholt, J.A. (2015). Extra Cytoplasmic Function sigma factors, recent structural insights into promoter recognition and regulation. Curr. Opin. Struct. Biol. *30*, 71–78.

Campbell, E.A., Masuda, S., Sun, J.L., Muzzin, O., Olson, C.A., Wang, S., and Darst, S.A. (2002). Crystal structure of the Bacillus stearothermophilus anti-σ factor SpoIIAB with the sporulation σ factor sigmaF. Cell *108*, 795–807.

Chambers, J.R., Liao, J., Schurr, M.J., and Sauer, K. (2014). BrlR from *Pseudomonas aeruginosa* is a c-di-GMP-responsive transcription factor. Mol. Microbiol. *92*, 471–487.

Chan, C., Paul, R., Samoray, D., Amiot, N.C., Giese, B., Jenal, U., and Schirmer, T. (2004). Structural basis of activity and allosteric control of diguanylate cyclase. Proc. Natl. Acad. Sci. USA *101*, 17084–17089.

Chater, K.F., Bruton, C.J., Plaskitt, K.A., Buttner, M.J., Méndez, C., and Helmann, J.D. (1989). The developmental fate of *S. coelicolor* hyphae depends upon a gene product homologous with the motility sigma factor of *B. subtilis*. Cell *59*, 133–143.

Chin, K.H., Lee, Y.C., Tu, Z.L., Chen, C.H., Tseng, Y.H., Yang, J.M., Ryan, R.P., McCarthy, Y., Dow, J.M., Wang, A.H., and Chou, S.H. (2010). The cAMP receptor-like protein CLP is a novel c-di-GMP receptor linking cell-cell signaling to virulence gene expression in *Xanthomonas campestris*. J. Mol. Biol. *396*, 646–662.

Chou, S.-H., and Galperin, M.Y. (2016). Diversity of cyclic di-GMP-binding proteins and mechanisms. J. Bacteriol. *198*, 32–46.

Christen, M., Christen, B., Folcher, M., Schauerte, A., and Jenal, U. (2005). Identification and characterization of a cyclic di-GMP-specific phosphodiesterase and its allosteric control by GTP. J. Biol. Chem. *280*, 30829–30837.

Crooks, G.E., Hon, G., Chandonia, J.M., and Brenner, S.E. (2004). WebLogo: a sequence logo generator. Genome Res. *14*, 1188–1190.

Datsenko, K.A., and Wanner, B.L. (2000). One-step inactivation of chromosomal genes in *Escherichia coli* K-12 using PCR products. Proc. Natl. Acad. Sci. USA *97*, 6640–6645.

den Hengst, C.D., Tran, N.T., Bibb, M.J., Chandra, G., Leskiw, B.K., and Buttner, M.J. (2010). Genes essential for morphological development and antibiotic production in *Streptomyces coelicolor* are targets of BldD during vegetative growth. Mol. Microbiol. *78*, 361–379.

Doublie, S. (1997). Preparation of selenomethionyl proteins for phase determination. Methods Enzymol. *276*, 523–530.

Dubey, B.N., Lori, C., Ozaki, S., Fucile, G., Plaza-Menacho, I., Jenal, U., and Schirmer, T. (2016). Cyclic di-GMP mediates a histidine kinase/phosphatase switch by noncovalent domain cross-linking. Sci. Adv. *2*, e1600823.

Duerig, A., Abel, S., Folcher, M., Nicollier, M., Schwede, T., Amiot, N., Giese, B., and Jenal, U. (2009). Second messenger-mediated spatiotemporal control of protein degradation regulates bacterial cell cycle progression. Genes Dev. *23*, 93–104.

Edgar, R.C. (2004). MUSCLE: multiple sequence alignment with high accuracy and high throughput. Nucleic Acids Res. *32*, 1792–1797.

Fazli, M., O'Connell, A., Nilsson, M., Niehaus, K., Dow, J.M., Givskov, M., Ryan, R.P., and Tolker-Nielsen, T. (2011). The CRP/FNR family protein Bcam1349 is a c-di-GMP effector that regulates biofilm formation in the respiratory pathogen *Burkholderia cenocepacia*. Mol. Microbiol. *82*, 327–341.

Feklístov, A., Sharon, B.D., Darst, S.A., and Gross, C.A. (2014). Bacterial sigma factors: a historical, structural, and genomic perspective. Annu. Rev. Microbiol. *68*, 357–376.

Flärdh, K., and Buttner, M.J. (2009). *Streptomyces* morphogenetics: dissecting differentiation in a filamentous bacterium. Nat. Rev. Microbiol. *7*, 36–49.

Flärdh, K., Findlay, K.C., and Chater, K.F. (1999). Association of early sporulation genes with suggested developmental decision points in *Streptomyces coelicolor* A3(2). Microbiology *145*, 2229–2243.

Flärdh, K., Richards, D.M., Hempel, A.M., Howard, M., and Buttner, M.J. (2012). Regulation of apical growth and hyphal branching in *Streptomyces*. Curr. Opin. Microbiol. *15*, 737–743.

Gautier, L., Cope, L., Bolstad, B.M., and Irizarry, R.A. (2004). affy–analysis of Affymetrix GeneChip data at the probe level. Bioinformatics *20*, 307–315.

Gibson, D.G., Young, L., Chuang, R.-Y., Venter, J.C., Hutchison, C.A., 3rd, and Smith, H.O. (2009). Enzymatic assembly of DNA molecules up to several hundred kilobases. Nat. Methods *6*, 343–345.

Gust, B., Challis, G.L., Fowler, K., Kieser, T., and Chater, K.F. (2003). PCR-targeted *Streptomyces* gene replacement identifies a protein domain needed for biosynthesis of the sesquiterpene soil odor geosmin. Proc. Natl. Acad. Sci. USA *100*, 1541–1546.

Gust, B., Chandra, G., Jakimowicz, D., Yuqing, T., Bruton, C.J., and Chater, K.F. (2004). λ red-mediated genetic manipulation of antibiotic-producing *Streptomyces*. Adv. Appl. Microbiol. *54*, 107–128.

Helmann, J.D. (1991). Alternative sigma factors and the regulation of flagellar gene expression. Mol. Microbiol. *5*, 2875–2882.

Helmann, J.D. (1999). Anti-sigma factors. Curr. Opin. Microbiol. *2*, 135–141.

Helmann, J.D., and Chamberlin, M.J. (1987). DNA sequence analysis suggests that expression of flagellar and chemotaxis genes in *Escherichia coli* and *Salmonella typhimurium* is controlled by an alternative sigma factor. Proc. Natl. Acad. Sci. USA *84*, 6422–6424.

Hengge, R. (2009). Principles of c-di-GMP signalling in bacteria. Nat. Rev. Microbiol. *7*, 263–273.

Hong, H.-J., Hutchings, M.I., Hill, L.M., and Buttner, M.J. (2005). The role of the novel Fem protein VanK in vancomycin resistance in *Streptomyces coelicolor*. J. Biol. Chem. *280*, 13055–13061.

Hopwood, D.A. (2007). *Streptomyces* in nature and medicine: the antibiotic makers (New York, NY: Oxford University Press).

Hsueh, Y.H., Cozy, L.M., Sham, L.T., Calvo, R.A., Gutu, A.D., Winkler, M.E., and Kearns, D.B. (2011). DegU-phosphate activates expression of the anti-sigma factor FlgM in *Bacillus subtilis*. Mol. Microbiol. *81*, 1092–1108.

Hughes, K.T., and Mathee, K. (1998). The anti-sigma factors. Annu. Rev. Microbiol. *52*, 231–286.

Hughes, K.T., Gillen, K.L., Semon, M.J., and Karlinsey, J.E. (1993). Sensing structural intermediates in bacterial flagellar assembly by export of a negative regulator. Science *262*, 1277–1280.

Hull, T.D., Ryu, M.H., Sullivan, M.J., Johnson, R.C., Klena, N.T., Geiger, R.M., Gomelsky, M., and Bennett, J.A. (2012). Cyclic Di-GMP phosphodiesterases RmdA and RmdB are involved in regulating colony morphology and development in *Streptomyces coelicolor*. J. Bacteriol. *194*, 4642–4651.

Jenal, U., Reinders, A., and Lori, C. (2017). Cyclic di-GMP: second messenger extraordinaire. Nat. Rev. Microbiol. *15*, 271–284.

Jones, T.A., Zou, J.-Y., Cowan, S.W., and Kjeldgaard, M. (1991). Improved methods for building protein models in electron density maps and the location of errors in these models. Acta Crystallogr. A *47*, 110–119.

Karimova, G., Pidoux, J., Ullmann, A., and Ladant, D. (1998). A bacterial two-hybrid system based on a reconstituted signal transduction pathway. Proc. Natl. Acad. Sci. USA *95*, 5752–5756.

Kieser, T., Bibb, M.J., Buttner, M.J., Chater, K.F., and Hopwood, D.A. (2000). Practical Streptomyces Genetics (Norwich: The John Innes Foundation).

Krasteva, P.V., Fong, J.C., Shikuma, N.J., Beyhan, S., Navarro, M.V., Yildiz, F.H., and Sondermann, H. (2010). *Vibrio cholerae* VpsT regulates matrix production and motility by directly sensing cyclic di-GMP. Science *327*, 866–868.

Kudo, N., Kimura, M., Beppu, T., and Horinouchi, S. (1995). Cloning and characterization of a gene involved in aerial mycelium formation in *Streptomyces griseus*. J. Bacteriol. *177*, 6401–6410.

Lambert, L.J., Wei, Y., Schirf, V., Demeler, B., and Werner, M.H. (2004). T4 AsiA blocks DNA recognition by remodeling σ^{70} region 4. EMBO J. *23*, 2952–2962.

Latoscha, A., Wörmann, M.E., and Tschowri, N. (2019). Nucleotide second messengers in *Streptomyces*. Microbiology *165*, 1153–1165.

Leduc, J.L., and Roberts, G.P. (2009). Cyclic di-GMP allosterically inhibits the CRP-like protein (Clp) of *Xanthomonas axonopodis* pv. citri. J. Bacteriol. *191*, 7121–7122.

Lee, V.T., Matewish, J.M., Kessler, J.L., Hyodo, M., Hayakawa, Y., and Lory, S. (2007). A cyclic-di-GMP receptor required for bacterial exopolysaccharide production. Mol. Microbiol. *65*, 1474–1484.

Leslie, A.G. (2006). The integration of macromolecular diffraction data. Acta Crystallogr. D Biol. Crystallogr. *62* (Pt 1), 48–57.

Li, W., and He, Z.-G. (2012). LtmA, a novel cyclic di-GMP-responsive activator, broadly regulates the expression of lipid transport and metabolism genes in *Mycobacterium smegmatis*. Nucleic Acids Res. *40*, 11292–11307.

Li, W., Hu, L., Xie, Z., Xu, H., Li, M., Cui, T., and He, Z.-G. (2018a). Cyclic di-GMP integrates functionally divergent transcription factors into a regulation pathway for antioxidant defense. Nucleic Acids Res. *46*, 7270–7283.

Li, W., Li, M., Hu, L., Zhu, J., Xie, Z., Chen, J., and He, Z.-G. (2018b). HpoR, a novel c-di-GMP effective transcription factor, links the second messenger's regulatory function to the mycobacterial antioxidant defense. Nucleic Acids Res. *46*, 3595–3611.

Little, R.H., Grenga, L., Saalbach, G., Howat, A.M., Pfeilmeier, S., Trampari, E., and Malone, J.G. (2016). Adaptive remodeling of the bacterial proteome by specific ribosomal modification regulates *Pseudomonas* infection and niche colonisation. PLoS Genet. *12*, e1005837.

Liu, G., Chater, K.F., Chandra, G., Niu, G., and Tan, H. (2013). Molecular regulation of antibiotic biosynthesis in *streptomyces*. Microbiol. Mol. Biol. Rev. *77*, 112–143.

Lori, C., Ozaki, S., Steiner, S., Böhm, R., Abel, S., Dubey, B.N., Schirmer, T., Hiller, S., and Jenal, U. (2015). Cyclic di-GMP acts as a cell cycle oscillator to drive chromosome replication. Nature *523*, 236–239.

Lovering, A.L., Capeness, M.J., Lambert, C., Hobley, L., and Sockett, R.E. (2011). The structure of an unconventional HD-GYP protein from *Bdellovibrio* reveals the roles of conserved residues in this class of cyclic-di-GMP phosphodiesterases. MBio *2*, e00163–e11.

Matsuyama, B.Y., Krasteva, P.V., Baraquet, C., Harwood, C.S., Sondermann, H., and Navarro, M.V.A.S. (2016). Mechanistic insights into c-di-GMP-dependent control of the biofilm regulator FleQ from *Pseudomonas aeruginosa*. Proc. Natl. Acad. Sci. USA *113*, E209–E218.

McCormick, J.R., and Flärdh, K. (2012). Signals and regulators that govern *Streptomyces* development. FEMS Microbiol. Rev. *36*, 206–231.

Morgan, J.L.W., McNamara, J.T., and Zimmer, J. (2014). Mechanism of activation of bacterial cellulose synthase by cyclic di-GMP. Nat. Struct. Mol. Biol. *21*, 489–496.

Newell, P.D., Monds, R.D., and O'Toole, G.A. (2009). LapD is a bis-(3′,5′)-cyclic dimeric GMP-binding protein that regulates surface attachment by *Pseudomonas fluorescens* Pf0-1. Proc. Natl. Acad. Sci. USA *106*, 3461–3466.

Newell, P.D., Boyd, C.D., Sondermann, H., and O'Toole, G.A. (2011). A c-di-GMP effector system controls cell adhesion by inside-out signaling and surface protein cleavage. PLoS Biol. *9*, e1000587.

Paget, M.S. (2015). Bacterial sigma factors and anti-sigma factors: Structure, function and distribution. Biomolecules *5*, 1245–1265.

Paget, M.S., Chamberlin, L., Atrih, A., Foster, S.J., and Buttner, M.J. (1999). Evidence that the extracytoplasmic function sigma factor sigmaE is required for normal cell wall structure in Streptomyces coelicolor A3(2). J. Bacteriol. *181*, 204–211.

Patikoglou, G.A., Westblade, L.F., Campbell, E.A., Lamour, V., Lane, W.J., and Darst, S.A. (2007). Crystal structure of the *Escherichia coli* regulator of σ^{70}, Rsd, in complex with σ^{70} domain 4. J. Mol. Biol. *372*, 649–659.

Paul, R., Weiser, S., Amiot, N.C., Chan, C., Schirmer, T., Giese, B., and Jenal, U. (2004). Cell cycle-dependent dynamic localization of a bacterial response regulator with a novel di-guanylate cyclase output domain. Genes Dev. *18*, 715–727.

Qi, Y., Chuah, M.L., Dong, X., Xie, K., Luo, Z., Tang, K., and Liang, Z.X. (2011). Binding of cyclic diguanylate in the non-catalytic EAL domain of FimX induces a long-range conformational change. J. Biol. Chem. *286*, 2910–2917.

Raju, H., and Sharma, R. (2017). Crystal structure of BrlR with c-di-GMP. Biochem. Biophys. Res. Commun. *490*, 260–264.

Roelofs, K.G., Jones, C.J., Helman, S.R., Shang, X., Orr, M.W., Goodson, J.R., Galperin, M.Y., Yildiz, F.H., and Lee, V.T. (2015). Systematic identification of cyclic-di-GMP binding proteins in *Vibrio cholerae* reveals a novel class of cyclic-di-GMP-binding ATPases associated with type II secretion systems. PLoS Pathog. *11*, e1005232.

Ross, P., Weinhouse, H., Aloni, Y., Michaeli, D., Weinberger-Ohana, P., Mayer, R., Braun, S., de Vroom, E., van der Marel, G.A., van Boom, J.H., and Benziman, M. (1987). Regulation of cellulose synthesis in *Acetobacter xylinum* by cyclic diguanylic acid. Nature *325*, 279–281.

Ryan, R.P., Fouhy, Y., Lucey, J.F., Crossman, L.C., Spiro, S., He, Y.W., Zhang, L.H., Heeb, S., Cámara, M., Williams, P., and Dow, J.M. (2017). Retraction. Proc. Natl. Acad. Sci. USA *114*, E7031.

Ryding, N.J., Kelemen, G.H., Whatling, C.A., Flärdh, K., Buttner, M.J., and Chater, K.F. (1998). A developmentally regulated gene encoding a repressor-like protein is essential for sporulation in *Streptomyces coelicolor* A3(2). Mol. Microbiol. *29*, 343–357.

Ryjenkov, D.A., Simm, R., Römling, U., and Gomelsky, M. (2006). The PilZ domain is a receptor for the second messenger c-di-GMP: the PilZ domain protein YcgR controls motility in enterobacteria. J. Biol. Chem. *281*, 30310–30314.

Schirmer, T., and Jenal, U. (2009). Structural and mechanistic determinants of c-di-GMP signalling. Nat. Rev. Microbiol. *7*, 724–735.

Schlimpert, S., Flärdh, K., and Buttner, M.J. (2016). Fluorescence time-lapse imaging of the complete *Streptomyces* life cycle using a microfluidic device. J. Vis. Exp. *108*, e53863.

Schlimpert, S., Wasserstrom, S., Chandra, G., Bibb, M.J., Findlay, K.C., Flärdh, K., and Buttner, M.J. (2017). Two dynamin-like proteins stabilize FtsZ rings during *Streptomyces* sporulation. Proc. Natl. Acad. Sci. USA *114*, E6176–E6183.

Schmidt, A.J., Ryjenkov, D.A., and Gomelsky, M. (2005). The ubiquitous protein domain EAL is a cyclic diguanylate-specific phosphodiesterase: enzymatically active and inactive EAL domains. J. Bacteriol. *187*, 4774–4781.

Schumacher, M.A., and Zeng, W. (2016). Structures of the activator of *K. pneumonia* biofilm formation, MrkH, indicates PilZ domains involved in c-di-GMP and DNA binding. Proc. Natl. Acad. Sci. USA *113*, 10067–10072.

Schumacher, M.A., Zeng, W., Findlay, K.C., Buttner, M.J., Brennan, R.G., and Tschowri, N. (2017). The *Streptomyces* master regulator BldD binds c-di-GMP sequentially to create a functional $BldD_2$-$(c\text{-}di\text{-}GMP)_4$ complex. Nucleic Acids Res. *45*, 6923–6933.

Schumacher, M.A., Bush, M.J., Bibb, M.J., Ramos-León, F., Chandra, G., Zeng, W., and Buttner, M.J. (2018). The crystal structure of the RsbN-σBldN complex from Streptomyces venezuelae defines a new structural class of anti-σ factor. Nucleic Acids Res. *46*, 7405–7417.

Skotnicka, D., Smaldone, G.T., Petters, T., Trampari, E., Liang, J., Kaever, V., Malone, J.G., Singer, M., and Søgaard-Andersen, L. (2016). A minimal threshold of c-di-GMP is essential for fruiting body formation and sporulation in *Myxococcus xanthus*. PLoS Genet. *12*, e1006080.

Smyth, G.K. (2005). Limma: linear models for microarray data. In Bioinformatics and Computational Biology Solutions using R and Bioconductor, R. Gentleman, V. Carey, S. Dudoit, R. Irizarry, and W. Huber, eds. (New York: Springer), pp. 397–420.

Sorenson, M.K., and Darst, S.A. (2006). Disulfide cross-linking indicates that FlgM-bound and free σ^{28} adopt similar conformations. Proc. Natl. Acad. Sci. USA *103*, 16722–16727.

Sorenson, M.K., Ray, S.S., and Darst, S.A. (2004). Crystal structure of the flagellar sigma/anti-sigma complex sigma(28)/FlgM reveals an intact sigma factor in an inactive conformation. Mol. Cell *14*, 127–138.

Srivastava, D., Harris, R.C., and Waters, C.M. (2011). Integration of cyclic di-GMP and quorum sensing in the control of *vpsT* and *aphA* in *Vibrio cholerae*. J. Bacteriol. *193*, 6331–6341.

Srivastava, D., Hsieh, M.-L., Khataokar, A., Neiditch, M.B., and Waters, C.M. (2013). Cyclic di-GMP inhibits *Vibrio cholerae* motility by repressing induction of transcription and inducing extracellular polysaccharide production. Mol. Microbiol. *90*, 1262–1276.

Steiner, S., Lori, C., Boehm, A., and Jenal, U. (2013). Allosteric activation of exopolysaccharide synthesis through cyclic di-GMP-stimulated protein-protein interaction. EMBO J. *32*, 354–368.

Sudarsan, N., Lee, E.R., Weinberg, Z., Moy, R.H., Kim, J.N., Link, K.H., and Breaker, R.R. (2008). Riboswitches in eubacteria sense the second messenger cyclic di-GMP. Science *321*, 411–413.

Trampari, E., Stevenson, C.E.M., Little, R.H., Wilhelm, T., Lawson, D.M., and Malone, J.G. (2015). Bacterial rotary export ATPases are allosterically regulated by the nucleotide second messenger cyclic-di-GMP. J. Biol. Chem. *290*, 24470–24483.

Tran, N.T., Den Hengst, C.D., Gomez-Escribano, J.-P., and Buttner, M.J. (2011). Identification and characterization of CdgB, a diguanylate cyclase involved in developmental processes in *Streptomyces coelicolor*. J. Bacteriol. *193*, 3100–3108.

Tschowri, N. (2016). Cyclic dinucleotide-controlled regulatory pathways in *Streptomyces* species. J. Bacteriol. *198*, 47–54.

Tschowri, N., Schumacher, M.A., Schlimpert, S., Chinnam, N.B., Findlay, K.C., Brennan, R.G., and Buttner, M.J. (2014). Tetrameric c-di-GMP mediates effective transcription factor dimerization to control *Streptomyces* development. Cell *158*, 1136–1147.

van Wezel, G.P., and McDowall, K.J. (2011). The regulation of the secondary metabolism of *Streptomyces*: new links and experimental advances. Nat. Prod. Rep. *28*, 1311–1333.

Wang, F., He, Q., Su, K., Gao, F., Huang, Y., Lin, Z., Zhu, D., and Gu, L. (2016). The PilZ domain of MrkH represents a novel DNA binding motif. Protein Cell *7*, 766–772.

Wei, Z., Chen, C., Liu, Y.J., Dong, S., Li, J., Qi, K., Liu, S., Ding, X., Ortiz de Ora, L., Muñoz-Gutiérrez, I., et al. (2019). Alternative σ^{I}/anti-σ^{I} factors represent a unique form of bacterial σ/anti-σ complex. Nucleic Acids Res. *47*, 5988–5997.

Yonekawa, T., Ohnishi, Y., and Horinouchi, S. (1999). Involvement of *amfC* in physiological and morphological development in *Streptomyces coelicolor* A3(2). Microbiology *145*, 2273–2280.

STAR★METHODS

KEY RESOURCES TABLE

REAGENT or RESOURCE	SOURCE	IDENTIFIER
Antibodies		
Rabbit polyclonal anti-σ^{WhiG}	Cambridge Research Biochemicals	Custom made
Rabbit polyclonal anti-RsiG	Cambridge Research Biochemicals	Custom made
Bacterial and Virus Strains		
Please refer to Table S3		N/A
Chemicals, Peptides, and Recombinant Proteins		
OCT Compound	Agar Scientific Ltd	Cat#AGR1180
cOmplete, Mini, EDTA-free Protease Inhibitor Cocktail	Roche Applied Science	Cat#11836170001
Protein A–Sepharose	Sigma	Cat#P3391
Cobalt resin	Takara Bio USA	Cat#635504
Proteinase K	Roche	Cat#RPROTK-RO
TRIzol	Invitrogen	Cat#15596026
GeneChip array	Affymetrix	*Streptomyces* diS_div712a
SuperScript II reverse transcriptase	Invitrogen	Cat#18064-014
Random Primers	Invitrogen	Cat#48190011
Bradford Reagent	Biorad	Cat#500-0006
2′- O- (6- [DY-505-05]- aminohexylcarbamoyl))guanosine- 3′, 5′- cyclic monophosphate (2′-[DY505-05]-AHC-cGMP)	BioLog	Cat#D135-001
2′- O- (6- [DY-505-05]- aminohexylcarbamoyl))guanosine- 3′, 5′- cyclic monophosphate (2′-[DY505-05]-AHC-cAMP), sodium salt	BioLog	Cat#C195-001
Critical Commercial Assays		
QIAquick PCR Purification Kit	QIAGEN	Cat#28104
RNeasy Mini Kit	QIAGEN	Cat#74104
TURBO DNA-*free* Kit	Ambion	Cat#AM1907
SensiFAST SYBR No-ROX kit	Bioline	Cat#BIO-98005
Anti-Rabbit Detection Module for Jess, Wes, Peggy Sue or Sally Sue	ProteinSimple	Cat#DM-001
12-230 kDa Jess or Wes Separation Module, 8 × 25 capillary cartridges	ProteinSimple	Cat#SM-W004
Deposited Data		
Crystal Structures	This paper	PDB: 6PFJ and PDB: 6PFV
ChIP-seq data	This paper	E-MTAB-8160 (ArrayExpress)
Microarray transcriptional profiling data	This paper	E-MTAB-8114 (ArrayExpress)
Oligonucleotides		
Please refer to Table S3		N/A
Recombinant DNA		
Please refer to Table S3		N/A
Software and Algorithms		
Fiji	open-source software package	http://fiji.sc/
Prism	Graphpad	https://www.graphpad.com/scientific-software/prism/

LEAD CONTACT AND MATERIALS AVAILABLITY

The Lead Contact is Mark Buttner (mark.buttner@jic.ac.uk). All stable reagents generated in this study are available from the Lead Contact with a completed Materials Transfer Agreement.

EXPERIMENTAL MODEL AND SUBJECT DETAILS

For details about the bacterial strains and culture conditions, please refer to the strain list (Table S3) and Method Details.

METHOD DETAILS

Bacterial strains, plasmids, media, and conjugations

Strains, plasmids, and oligonucleotides used in this study are listed in Table S3. *Escherichia coli* strain DH5α was used for plasmid and cosmid propagation. Disruption cosmids were generated using *E. coli* strain BW25113 (Datsenko and Wanner, 2000) carrying a λ RED plasmid, pIJ790. The *dam dsm hsdS E. coli* strain ET12576 containing pUZ8002 (Paget et al., 1999) was used to conjugate cosmids and plasmids into *S. venezuelae* (Kieser et al., 2000; Bibb et al., 2012). *E. coli* strains were grown on LB or LB agar at 37°C. *S. venezuelae* strains were typically grown in liquid or solid MYM media supplemented with trace element solution (Bibb et al., 2012) but the hypersporulation phenotype was examined on Difco Nutrient Agar (DNA) or in Difco Nutrient Broth (DNB), where this phenotype is strongest. Where required for selection, the following antibiotics were added to growth media: 50 μg/mL apramycin, 100 μg/mL carbenicillin, 25 μg/mL chloramphenicol, 25 μg/mL hygromycin, and/or 50 μg/mL kanamycin.

Construction and complementation of S. venezuelae null mutants

The *whiG*, *vnz15005*, and *rsiG* null mutants were generated using the Redirect PCR targeting system (Gust et al., 2003, 2004). A cosmid library that covers > 98% of the *S. venezuelae* genome has been constructed and is fully documented at http://strepdb.streptomyces.org.uk/. Cosmid Sv-6_E12 (contains *whiG*), Pl2_H19 (contains *vnz15005*), or Sv-2_C01 (contains *rsiG*) was introduced to *E. coli* strain BW25113 containing pIJ790 and *whiG*, *vnz15005*, or *rsiG* was replaced with the *apr-oriT* cassette amplified from pIJ773 using primer pairs vnz26215_redi_F and vnz26215_redi_R, vnz15005_redi_F and vnz15005_redi_R, or vnz19430_redi_F and vnz19430_redi_R. Null mutants were confirmed by PCR analysis using the flanking primer sets vnz26215_check_F and vnz26215_check_R, vnz15005_check_F and vnz15005_check_R, or vnz19430_check_F and vnz19430_check_R. Complementation of the *whiG* and *rsiG* null mutants was achieved by amplifying the coding region and native promoter of each gene using the primer sets vnz26215_comp_F and vnz26215_comp_R, or vnz19430_comp_F and vnz19430_comp_R and cloning each fragment into HindIII/Asp718-cut pIJ10770 (Schlimpert et al., 2017) to generate plasmids pIJ10900 and pIJ10901. Complementation of the *rsiG* null mutant with the *rsiG** allele was accomplished by gene synthesis of *rsiG** (GenScript), with identical promoter and coding sequence to that found in pIJ10901 except for the four mutated codons. The *rsiG** allele was subsequently cloned into HindIII/Asp718-cut pIJ10770 to generate pIJ10913. Complementation plasmids were introduced into *S. venezuelae* null mutants by conjugation.

Overexpression of proteins in S. venezuelae

The coding region of *whiG* was amplified using primer set vnz26215_ermE_F and vnz26215_ermE_R. The PCR product was cloned into NdeI/HindIII-cut pIJ10257 (Hong et al., 2005) to generate plasmid pIJ10902. This construction results in *whiG* being placed under the control of the strong constitutive *ermE** promoter.

For overexpression of both WhiH and WhiI together, the coding regions of both genes were amplified with primers HI_ermE_P1and HI_ermE_P2 (for *whiH*) HI_ermE_P3 and HI_ermE_P4 (for *whiI)*. Both genes, separated by a short spacer containing a ribosome binding site, were then inserted into NdeI/HindIII-digested pIJ10257 by Gibson Assembly (Gibson et al., 2009). This resulted in the creation of plasmid pIJ10906, which contains *whiH* and *whiI* under the control of the same *ermE** promoter. All overexpression plasmids were introduced into WT *S. venezuelae* or the *ΔwhiG* mutant by conjugation.

Scanning Electron Microscopy

Colonies were mounted on the surface of an aluminum stub with optimal cutting temperature compound (Agar Scientific Ltd, Essex, UK), plunged into liquid nitrogen slush at approximately −210°C to cryopreserve the material, and transferred to the cryostage of an Alto 2500 cryotransfer system (Gatan, Oxford, England) attached to a FEI NanoSEM 450 field emission gun scanning electron microscope (FEI Ltd, Eindhoven, the Netherlands). The surface frost was sublimated at −95°C for 3½ min before the sample was sputter coated with platinum for 2 min at 10 mA at below −110°C. Finally, the sample was moved onto the cryostage in the main chamber of the microscope, held at approximately −130°C, and viewed at 3 kV.

Chromatin immunoprecipitation, library construction, sequencing, and ChIP-seq data analysis

WT *S. venezuelae* and the *ΔwhiG* null mutant (negative control) were grown in 30 mL volumes of MYM. During mid-sporulation, formaldehyde was added to cultures at a final concentration of 1% (v/v) and incubation was continued for 30 min. Glycine was then added

to a final concentration of 125 mM to stop the cross-linking. Cultures were left at room temperature (RT) for 5 min before the mycelium was harvested and washed twice in PBS buffer (pH 7.4). Each mycelial pellet was resuspended in 0.75 mL lysis buffer (10 mM Tris HCl pH 8.0, 50 mM NaCl) containing 10 mg/mL lysozyme and protease inhibitor (Roche Applied Science) and incubated at 37°C for 25 min. An equal volume of IP buffer (100 mM Tris HCl pH 8, 250 mM NaCl, 0.5% Triton X-100, 0.1% SDS) containing protease inhibitor was added and samples were chilled on ice. Samples were sonicated for 8 cycles of 20 s each at 8 microns to shear the chromosomal DNA into fragments ranging from 300-1000 bp in size. Samples were centrifuged twice at 13,000 rpm at 4°C for 10 min to clear the cell extract. The supernatant was incubated with 10% (v/v) protein A-Sepharose (Sigma) for 1 h on a rotating wheel to remove non-specifically binding proteins. Samples were then centrifuged for 15 min at 4°C and 13,000 rpm to remove the beads. Supernatants were incubated with 10% (v/v) anti-σ^{WhiG} polyclonal antibody overnight at 4°C with rotation. Subsequently, 10% (v/v) protein A-Sepharose was added to precipitate σ^{WhiG} and incubation was continued for 4 hr. Samples were centrifuged at 4°C and 3500 rpm for 5 min and the pellets were washed twice with 0.5x IP buffer, and then twice with 1x IP buffer. Each pellet was incubated overnight at 65°C in 150 μl IP elution buffer (50 mM Tris HCl pH 7.6, 10 mM EDTA, 1% SDS) to reverse cross-links. Samples were centrifuged at 13,000 rpm for 5 min to remove the beads. Each pellet was re-extracted with 50 μl TE buffer (10 mM Tris HCl pH 7.4, 1 mM EDTA) and the supernatant incubated with 0.2 mg/mL Proteinase K (Roche) for 2 h at 55°C. The resulting samples were extracted with phenol-chloroform and further purified using QiaQuick columns, eluting in 50 μL EB buffer (QIAGEN). Library construction and sequencing were performed by the Earlham Institute, Norwich Research Park, Norwich, United Kingdom.

The reads in the fastq files received from the sequencing contractor were aligned to the *S. venezuelae* genome (GenBank: CP018074) using the bowtie2 software (version 2.2.9), which resulted in one SAM (.sam) file for each fastq file (single ended sequencing). For each sam file, the *depth* command of *samtools* (version 1.8) was used to arrive at the depth of sequencing at each nucleotide position of the *S. venezuelae* chromosome (https://www.sanger.ac.uk/science/tools/samtools-bcftools-htslib). From the sequencing depths at each nucleotide position determined in step 2, a local enrichment was calculated in a moving window of 30 nucleotides moving in steps of 15 nucleotides as (the mean depth at each nucleotide position in the 30-nucleotide window) divided by (the mean depth at each nucleotide position in a 3000-nucleotide window centered around the 30-nucleotide window).This results in an enrichment ratio value for every 15 nucleotides along the genome. Local enrichment in total (non-IP) samples were subtracted from those in IP samples. Enrichment for the control samples (*whiG* deletion strain) was subtracted from the enrichment in corresponding WT samples. Significance of enrichment values were calculated assuming normal distribution of the enrichment values. Genomic positions were ordered from low to high P values. Association of regions of enrichment with P values below 1e-4 with genes on the chromosome was done by simply listing genes left and right of the region. Rows of lower significance with the same context of genes were removed to leave the most significant row for each combination of left, right and *within* genes. Genes had to be in the right orientation and within 500 nucleotides of the enriched region for association with the region.

Microarray analysis

WT *S. venezuelae* and the *ΔwhiG* null mutant were grown in triplicate 30 mL volumes of MYM and samples were collected at 2 h intervals from 8 to 20 h (26 mL at 8 h, 9 mL at 10 h, and 6 mL at subsequent time points). A 300 μL sample was removed at each time point to check the stage of development by phase contrast light microscopy, and to measure the optical density. Cells were harvested by centrifugation at 4°C, frozen in dry ice/ethanol, and ground in liquid nitrogen in a mortar and pestle that had been chilled in a dry ice/liquid nitrogen bath. Ground material was suspended in 2 mL TRIzol (Invitrogen) and divided equally between two 2 mL tubes; one was stored at −80°C as a backup and the other used for RNA isolation. Total RNA was isolated using the RNeasy mini kit (QIAGEN), largely according to the manufacturer's instructions, but with several modifications. Cell pellets were resuspended in TE buffer containing 15 mg/mL lysozyme and incubated for 60 min at room temperature. After addition of RNeasy RLT buffer samples were sonicated for 3 cycles of 20 s (Sanyo Soniprep 150, amplitude 18 microns), resting on ice for 1 min between bursts, then extracted twice with phenol-chloroform and once with chloroform. Extracts were then treated with ethanol and applied to the RNeasy mini columns for purification according to the supplied protocol, including an on-column DNaseI digestion step for 60 min at room temperature. Purified RNA was finally eluted in 300 μL RNase-free water. Single-strand reverse transcription (amplification) and indirect labeling of 10 μg total RNA were performed for hybridization to *Streptomyces* diS_div712a GeneChip arrays according to the manufacturer's published protocol (Affymetrix). GeneChips were washed and stained using a GeneChip fluidics workstation model 450 and scanned with a Gene Array Scanner.

The CEL files received from the scanner were read into the R package for statistical computing (http://www.R-project.org/) using the *ReadAffy* function of the *affy* package (Gautier et al., 2004). The *rma* function of the *affy* package was used to compute an *ExpressionSet* object from the CEL files. This *ExpressionSet* object contains the expression values (log2) for each gene in each CEL file. The function *lmFit* of the limma package (Smyth, 2005), along with a suitable design matrix, was used to combine replicate arrays into single coefficients of expressions for each gene at each time point or strain into an *MArrayLM* object. Expression values were retrieved from the *MArrayLM* object and used to generate the graphs shown in this paper.

qRT-PCR

Mycelial pellets originating from 5 mL of culture grown in DNB medium were collected at appropriate time points, washed in PBS and resuspended in 900 μL lysis solution (400 μl phenol [pH4.3], 100 μL chloroform: isoamyl alcohol (24:1), and 400 μL RLT buffer [QIAGEN]) with lysing matrix B (MP Biomedicals) and homogenized using a FastPrep FP120 Cell Disruptor (Thermo Savant). Two

pulses of 30 s of intensity 6.0 were applied with cooling down for 90 s on ice between pulses. Supernatants were centrifuged for 15 min, full-speed on a bench-top centrifuge at 4°C and then treated according to the instructions given in the RNEasy Kit (QIAGEN), including an on-column DNase I digestion step. This was followed by an additional DNase I treatment (Turbo DNA-free, Ambion) until samples were free of DNA contamination (determined by PCR amplification of *hrdB*). For qRT-PCR, equal amounts (500 ng) of total RNA from each sample was converted to cDNA using SuperScript II reverse transcriptase and random primers (Invitrogen). cDNA was then used as a template in qRT-PCR using the SensiFAST SYBR No-ROX kit (Bioline). Three technical replicates were performed for each sample. Primers vnz28820_qRT_F and vnz28820_qRT_R were used to amplify the σ^{WhiG} target gene *whiI*, and primers hrdBqRT_F and hrdBqRT_R were used to amplify the *hrdB* reference gene. To normalize for differing primer efficiency, a standard curve was constructed using chromosomal DNA. Melting curve analysis was used to confirm the production of a specific single product from each primer pair. qRT-PCR was performed using a CFX96 Touch instrument using hardshell white PCR plates (BioRad), sealed with thermostable film covers (Thermo). PCR products were detected with SYBR green fluorescent dye and amplified according to the following protocol: 95°C, 3 min, then 45 cycles at 95°C 5 s, 62°C 10 s and 72°C 7 s. Melting curves were generated at 65 to 95°C with 0.5°C increments. The BioRad CFX manager software was used to calculate mean starting quantity (SQ) values for *whiI* at each time point. These values were divided by mean SQ values measured for *hrdB* at corresponding time points, resulting in relative expression values. Relative expression values were normalized against the mean relative expression value of the WT at 10 hr, which was set to 1. This experiment, including RNA isolation, was repeated once independently.

Western blotting

For analysis of protein levels, mycelial pellets originating from 5 mL of culture grown in DNB were resuspended in 2 mL of ice-cold wash buffer (20 mM Tris pH 8.0, 5 mM EDTA). Samples were centrifuged at 13,000 rpm for 1 min at 4°C. The supernatant was removed, and the pellet resuspended in 0.4 mL of sonication buffer (20 mM Tris pH 8.0, 5 mM EDTA, 1 x EDTA-free protease inhibitors [Roche]). Samples were sonicated at 4.5-micron amplitude for 7 rounds of 15 s, separated by 15 s of rest on ice. Lysed samples were then centrifuged at 13,000 rpm for 15 min at 4°C in order to remove cell debris. Total protein concentration was determined using a Bradford assay (Biorad). For analysis of RsiG or RsiG* levels, cell lysates were diluted to a final concentration of 0.7 mg/mL and loaded in triplicate into a microplate (ProteinSimple #043-165), along with a polyclonal anti-RsiG antibody raised in rabbit (Cambridge Biosciences) diluted 1:50. For analysis of σ^{WhiG} levels, cell lysates were diluted to a final concentration of 0.2 mg/mL and loaded in triplicate, along with a polyclonal anti- σ^{WhiG} antibody raised in rabbit diluted 1:50. For both cases, protein levels were analyzed using the automated Western Blotting machine Wes (ProteinSimple, San Jose, CA) with the Wes-Rabbit (12 to 230 kDa) Master kit according to the manufacturer's instructions.

Bacterial two-hybrid genomic library construction, screening, and analysis

Construction of bacterial two-hybrid genomic libraries was performed by BIO S&T (Saint-Laurent, Québec, Canada). Genomic DNA from *S. venezuelae* was sheared by sonication, then end-repaired and cloned into SmaI-digested pUT18C or pKT25. The ligation mix was transformed into competent DH10B *E. coli* cells and spread onto large agar plates, resulting in > 329,200 colonies (40X coverage, assuming an insert size of 1 kb) for each library. Colonies on each plate were washed into tubes, pooled, and plasmids purified by maxi-prep. For quality control, 8-12 clones were randomly selected from each library. All clones selected were found to contain inserts, and the average size of each insert was 2.6 kb in the pUT18C library and 2.2 kb in the pKT25 library.

To construct the 'bait' vector containing σ^{WhiG} fusions, the coding region of *whiG* was amplified using primer set vnz26215_BACTH_F and vnz26215_BACTH_R, and cloned into BACTH vectors (pKT25, pKNT25, pUT18, pUT18C) digested with XbaI and Asp718 to create plasmids pIJ10907-pIJ10910. Each *whiG*-containing bait vector was co-electroporated with 0.25 μL of a working stock (0.1-0.5 μg/μL) of the appropriate corresponding genomic library into electrocompetent *E. coli* strain BTH101. Prior to plating, transformants were washed twice in M63 minimal medium, followed by resuspension in 1 mL of M63. In order to ensure that transformation efficiency was sufficient to ensure screening of all possible interactions, the total number of transformants was measured by plating 1 μL onto an LB agar plate containing appropriate antibiotics. The remaining transformation mixture was plated onto M63 agar containing 0.3% lactose, 0.5 mM IPTG, 40 μg/mL X-gal, and appropriate antibiotics. Positive clones were re-tested on MacConkey agar containing 1% maltose and appropriate antibiotics. Plasmid DNA was then isolated from positive clones, and inserts sequenced using primer sets T18seq_F and T18seq_R, T25seq_F and T25seq_R, NT25seq_F and NT25seq_R, or T18Cseq_F and T18Cseq_R. Out-of-frame clones were excluded from further analysis.

To test the interaction of full-length RsiG with σ^{WhiG}, the coding sequence of *rsiG* was amplified using primers vnz19430_BACTH_F and vnz19430_BACTH_R and cloned into pKT25 and pUT18 vectors digested with XbaI and Asp718 to create plasmids pIJ10911 and pIJ10912. *E. coli* BTH101 was then co-transformed with 'T25' and 'T18' fusion plasmids. β-galactosidase activity was assayed in triplicate.

Overexpression and copurification of the σ^{WhiG} -RsiG complex

To coexpress His-tagged σ^{WhiG} and non-tagged RsiG, *whiG* flanked by a 5′ EcoRI site and a 3′ HindIII site was amplified using primer set vnz26215_MCS1_F and vnz26215_MCS1_R, then cloned into multiple cloning site 1 (MCS1) of pCOLADuet-1. Next, *rsiG* flanked by a 5′ NdeI site and a 3′ KpnI site was amplified using primer set vnz19430_MCS2_F and vnz19430_MCS2_R and cloned into MCS2 of pCOLADuet-1 (with *whiG* already inserted at MCS1), resulting in the His-σ^{WhiG}/RsiG coexpression construct pIJ10914.

Coexpression plasmid pIJ10914 was introduced into *E. coli* BL21(DE3) pLysS Rosetta for protein expression. This strain was grown at 30°C in LB medium to an OD_{600} of 0.5, then induced with 0.25 mM IPTG and incubated overnight at 16°C. Cells were harvested by centrifugation, then resuspended in Buffer A (50 mM Tris-Cl pH 8.0, 200 mM NaCl, 5% glycerol), and disrupted with a high-pressure homogenizer (Avestin). Cell debris was then removed by centrifugation (15,000 rpm, 4°C, 45 min). The supernatant was loaded onto a HisTrap Excel 1 mL column using a Pharmacia Biotech FRAC-100 FPLC system and eluted using a 0-500 mM imidazole gradient in Buffer A over 20 min. Fractions were analyzed by SDS-PAGE.

Crystallization and structure determination of the σ^{WhiG}-RsiG complex

The RsiG-σ^{WhiG} coexpression system encoding both full length proteins failed to crystallize. Hence, several co-expression constructs of the RsiG-σ^{WhiG} complex were purified for crystallization trials. A construct (pIJ10915) in which full length σ^{WhiG} was expressed with an N-terminally truncated RsiG (Δ26 RsiG) with a cleavable N-terminal His-tag produced two crystal forms. Notably, the N-terminal ~50 residues are highly variable among the otherwise highly conserved RsiG homologs. For crystallization of this construct, the complex was purified similarly to the WT construct except cells were resuspended in a buffer (Buffer B) composed of 25 mM Tris-Cl pH 7.5, 300 mM NaCl, 5% glycerol. The supernatant was loaded onto a cobalt affinity column (Takara Bio USA) and the column washed with 300 mL of Buffer B. The protein complex was eluted using 100, 200, 300 and 500 mM imidazole steps. We later found that much longer washes with 1 l of Buffer B resulted in dissociation of the complex, which we realized stemmed from dissociation of the co-purifying c-di-GMP. For crystallization, the His-tag was removed from RsiG using a thrombin cleavage capture kit (Novagen, cat#69022-3FRZ) and the protein complex was concentrated to 40 mg/mL with buffer exchanges (in 25 mM Tris pH 7.5, 150 mM NaCl, 5% glycerol, 1 mM DTT) to remove the $CaCl_2$ present in the thrombin cleavage buffer. The complex was crystallized using the hanging drop vapor diffusion method at 22°C. Crystallization of the complex was effected by mixing the complex 1:1 with a solution composed of 0.1 M Tris Bicine pH 8.5, 0.03 M sodium nitrate, 0.03 M sodium phosphate, 0.03 M ammonium sulfate, 9% MPD, 10% PEG 1000 and 15% PEG 3350. Two crystal forms grew in the drops over a period of 1-3 months. The crystals were cryo-protected straight from the drop. Crystal form 1 takes the hexagonal space group, $P6_4$ with a = b = 92.1 Å, c = 96.6 Å and $\gamma = 120°$ while crystal form 2 is orthorhombic, $P22_12_1$, with a = 79.8 Å, b = 97.3 Å and c = 204.6 Å. The crystals were cryo-protected straight from the drop

Molecular replacement using the σ^{28} structure from the σ^{28}/FlgM complex failed. Hence, to obtain phase information, attempts were made to generate selenomethionone (semet) substituted σ^{WhiG}-RsiG complex using the methionine inhibitory pathway (Doublie, 1997). However, this approach failed as semet substituted σ^{WhiG} was not soluble (the semet σ^{WhiG} was found in inclusion bodies) even when the induction was performed at lower temperatures (4°-15°C). However, the semet RsiG, which harbors an N-terminal His-tag, was soluble and could be purified from the cell lysate using cobalt affinity chromatography (Takara Bio USA). Because the RsiG construct used only contains three methionines, we generated an RsiG mutant in which Leu56 and Leu85 were substituted to methionines (pIJ10919) to obtain enough signal to phase the σ^{WhiG}-RsiG complex. The semet substituted RsiG(L56M-L85M) protein was expressed at 15°C and the resultant cell pellet containing the induced protein was solubilized in 25 mM Tris-Cl pH 7.5, 300 mM NaCl, 5% glycerol. The cells were disrupted using a microfluidizer and the supernatant was loaded onto a cobalt affinity column (Takara Bio USA). The column was washed with 200 mL of the buffer and the protein eluted using 100, 200, 300 and 500 mM imidazole steps. The His-tag was removed from the semet RsiG(L56M-L85M) protein using a thrombin cleavage capture kit (Novagen, cat#69022-3FRZ). To generate non-semet σ^{WhiG} to form a complex with the semet RsiG(L56M-L85M) protein we utilized a construct in which σ^{WhiG} had a cleavable N-terminal His-tag (pIJ10920). The protein was expressed at 15°C overnight. The cells were solubilized in 25 mM Tris-Cl pH 7.5, 300 mM NaCl, 5% glycerol and the supernatant loaded onto a cobalt affinity column (Takara Bio USA). The column was washed with 300 mL of the buffer and σ^{WhiG} eluted with buffer B with 300 mM imidazole. The His-tag was removed from σ^{WhiG} using a thrombin cleavage capture kit (Novagen, cat#69022-3FRZ). To generate the complex, σ^{WhiG} was mixed 1:1 with RsiG(L56M-L85M) and subjected to size exclusion chromatography using a superdex 75 (S75) Sepharose column. A small amount of σ^{WhiG} -semetRsiG(L56M-L85M) complex was obtained and the complex crystallized using the same solution and conditions as the WT complex. Several σ^{WhiG}-semetRsiG(L56M-L85M) preparations were utilized in crystallization attempts but only one produced small crystals of the hexagonal form and one of these crystals was used to collect single wavelength anomalous diffraction (SAD) data to 2.7 Å at the Advanced Light Source (ALS) Beamline 8.3.1. Data for the WT crystals, hexagonal and orthorhombic, were also collected at ALS beamline 8.3.1. All X-ray intensity data were integrated in MOSFLM and scaled using SCALA (Leslie, 2006). Autosol in Phenix was used to locate heavy atoms sites with the semet SAD data, perform density modification and generate an initial electron density map. The model was built into the experimental SAD map using O (Jones et al., 1991) and minimally refined to an R_{free} of 31%. The c-di-GMP dimer was evident in this initial model. The structure contains one complex (one σ^{WhiG} and one RsiG) in the asymmetric unit (ASU). The partially refined model was then used in molecular replacement (MR) against the high-resolution hexagonal dataset. After multiple rounds of building in O and refinement with Phenix (Jones et al., 1991; Adams et al., 2010), the model converged to R_{work}/R_{free} values of 19.5%23.8% to 2.08 Å resolution. The final model includes RsiG residues 50-198 and σ^{WhiG} residues 24-183; 216-275, two c-di-GMP molecules and 60 solvent molecules.

The second crystal form contained three complexes in the ASU and the structure was solved by MR using Phaser with the 2.08 Å structure (minus the solvent and c-di-GMP) as the search model. Three clear solutions were obtained, and the structure was optimized by building in O and refinement in Phenix (Jones et al., 1991; Adams et al., 2010). Clear density for the same c-di-GMP dimer as in the hexagonal crystal form was observed in each of the three complexes after one round of refinement. After c-di-

GMP addition, and further refinement, the model converged to final R_{work}/R_{free} values of 20.9%/27.9% to 3.0 Å resolution. The final model includes RsiG residues 36-199 and σ^{WhiG} residues 24-183, 216-275 for one complex, RsiG residues 40-199 and σ^{WhiG} residues 24-183, 216-275 for the second complex and RsiG residues 41-199 in and σ^{WhiG} residues 24-183, 216-275 for the third structure. Each complex also contains an identically bound c-di-GMP dimer.

Determination of the affinity and specificity of c-di-GMP for RsiG and RsiG-σ^{WhiG} by fluorescence polarization (FP)

To measure c-di-GMP binding to RsiG and RsiG-σ^{WhiG}, 2′-O-(6-[Fluoresceinyl]aminohexylcarbamoyl)-cyclic diguanosine monophosphate (2′-Fluo-AHC-c-di-GMP) (BioLog), was used as a fluoresceinated reporter ligand. This molecule is conjugated via a 9-atom spacer to one of the 2′ hydroxyl groups of the c-di-GMP. This ligand was chosen as the structure shows that one ribose hydroxyl from each c-di-GMP would be solvent exposed when bound to RsiG and the RsiG-σ^{WhiG} complex. 2′-O-(6-[Fluoresceinyl]aminohexylcarbamoyl)-cyclic diadenosine monophosphate (2′-Fluo-AHC-c-di-AMP) (BioLog) was also used in binding studies to assess specificity of RsiG for c-di-GMP. The experiments were all carried out in a buffer of 150 mM NaCl and 25 mM Tris-HCl pH 7.5, which contained 1 nM 2′-Fluo-AHC-c-di-GMP or 2′-Fluo-AHC-c-di-AMP at 25°C. Increasing concentrations of RsiG alone (prepared using pIJ10917), or RsiG* alone (prepared using pIJ10918), or a mixture of equimolar concentrations of RsiG and σ^{WhiG}, were titrated into the reaction mixture to obtain their respective binding isotherms. The resultant data were plotted using KaleidaGraph and the curve fit to deduce binding affinities. Note, each batch of these *E. coli* produced proteins had some c-di-GMP contaminant, which efforts were made to remove, however, variability between batches was noted. Three technical repeats were performed for each curve and the standard errors from the three affinities were determined.

Time-lapse imaging of S. venezuelae

Cultures were grown in 30 mL DNB until fully differentiated (24-30 h). Before imaging, spores were prepared from the hypersporulating strain *S. venezuelae ermE*-whiG* by diluting the culture 1:50 in DNB medium. For all other strains, spores were prepared by centrifuging 1 mL of culture at 2000 rpm for 1 min, then diluting supernatant 1:20 in DNB medium. For all strains, 200 μL of prepared spores were loaded into the cell loading well of a prepared B04A microfluidic plate (Merck-Millipore). The ONIX manifold was then sealed to the B04A plate before transferring to the environmental chamber, pre-incubated at 30°C. Spores were loaded onto the plate at 8 psi for 5 s. Medium flow was set at 2 psi throughout the experiment, first with fresh DNB for 3 h, followed by sterile-filtered spent DNB medium derived from a shaking culture of *S. venezuelae* pKF351/pIJ10257.

Imaging was conducted using a Zeiss Axio Observer.Z1 widefield microscope equipped with a sCMOS camera (Hamamatsu Orca FLASH 4), a metal-halide lamp (HXP 120V), a hardware autofocus (Definitive Focus), a 96-well stage insert, an environmental chamber, a 100x 1.46 NA Oil DIC objective and the Zeiss 46 HE shift free (excitation500/25 nm, emission 535/30 nm) filter set (Schlimpert et al., 2016, 2017; Bush et al., 2017). Image collection began after clear signs of spore germination were observed (1-2 hr) and images were taken every 20 min. DIC images were captured with a 150 ms exposure time, YFP images were captured with a 350 ms exposure time. In all experiments, multiple x/y positions were imaged for each strain. Representative images were processed using the Fiji Software package (http://fiji.sc/; Schlimpert et al., 2016).

QUANTIFICATION AND STATISTICAL ANALYSIS

Prism software (GraphPad) was used for statistical analyses. Data in Figures 4B–4E and Figure 7D were derived from triplicates and are represented as mean ± Standard Error.

DATA AND CODE AVAILABILITY

The accession number for the ChIP-seq data reported in this paper is ArrayExpress: E-MTAB-8160. The accession number for the microarray transcriptional profiling data is ArrayExpress: E-MTAB-8114. The accession numbers for the crystal structures are PBD: 6PFJ, 6PFV.

Molecular Cell, Volume *77*

Supplemental Information

c-di-GMP Arms an Anti-σ to Control Progression of Multicellular Differentiation in *Streptomyces*

Kelley A. Gallagher, Maria A. Schumacher, Matthew J. Bush, Maureen J. Bibb, Govind Chandra, Neil A. Holmes, Wenjie Zeng, Max Henderson, Hengshan Zhang, Kim C. Findlay, Richard G. Brennan, and Mark J. Buttner

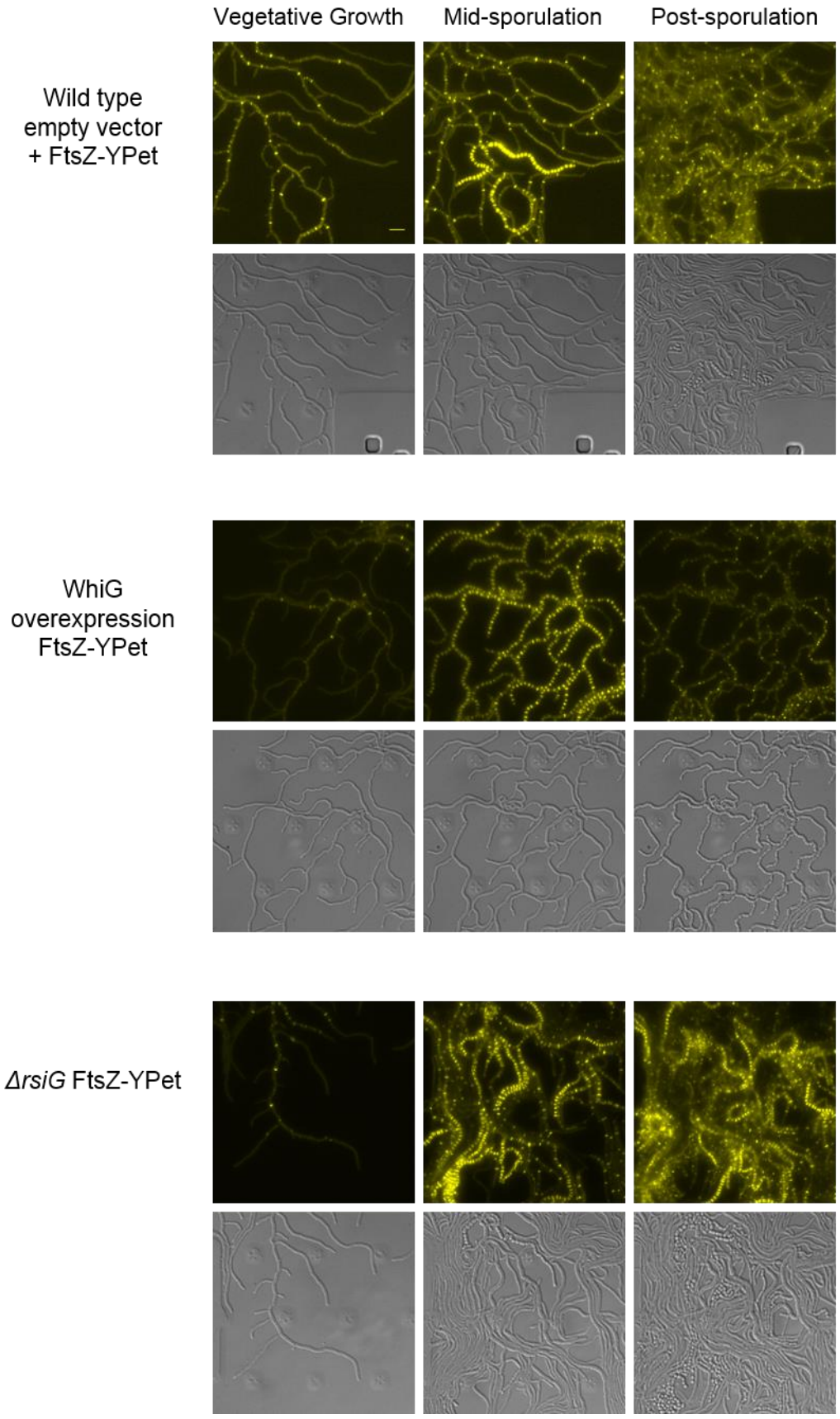

Figure S1. Overexpression of *whiG* or deletion of *rsiG* causes hypersporulation during growth in liquid culture, related to Figure 1 and Figure 4. Fluorescence (top) and DIC images (bottom) are stills taken from Movies S1-3. Scale bar = 5um.

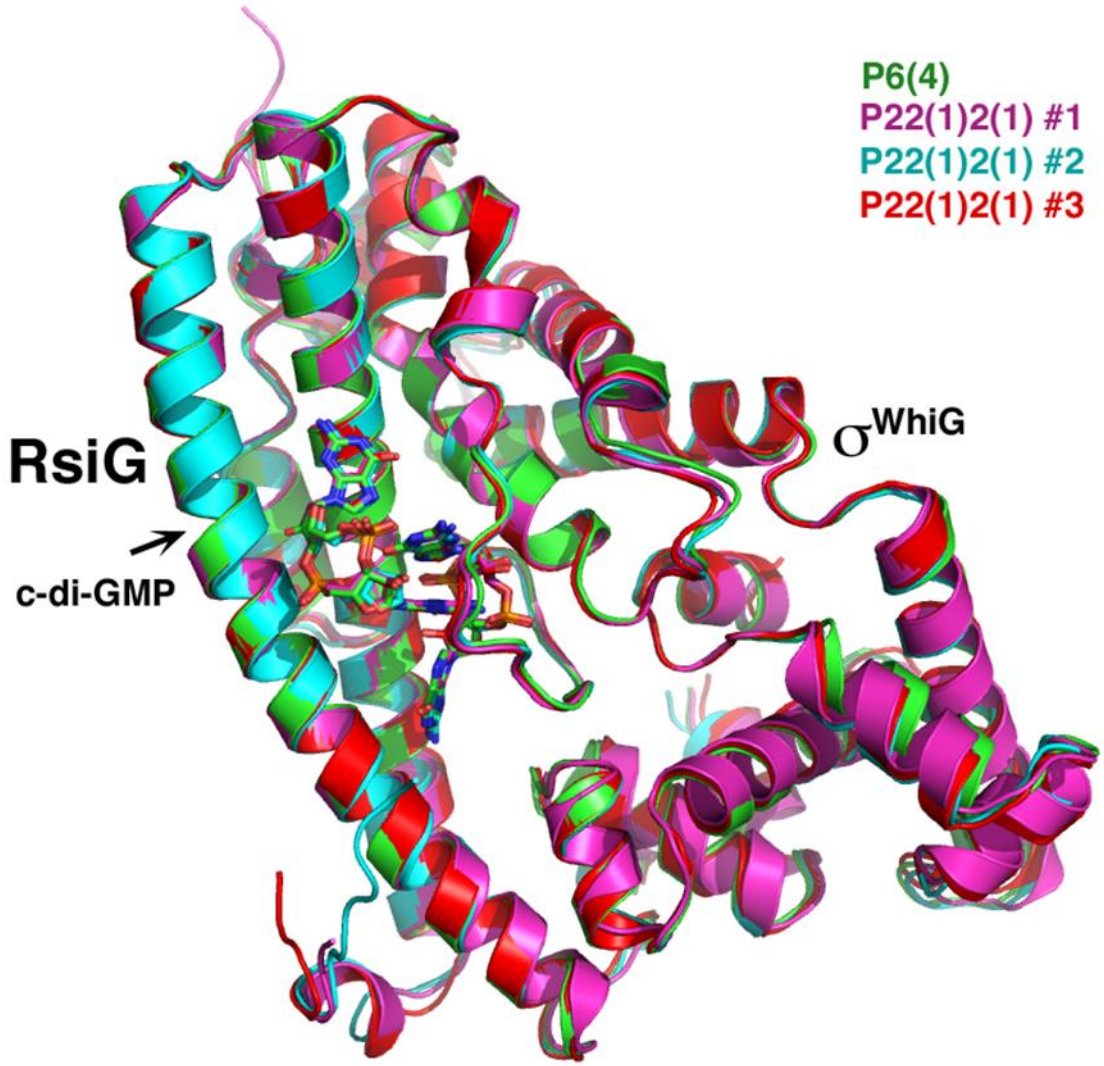

Figure S2. Superimposition of the two RsiG-σ^{WhiG} structures, related to Figure 5. The one complex in the crystallographic asymmetric unit (ASU) from the 2.08 Å structure (the hexagonal crystal form) is colored green and the three complexes in the ASU from the 3.0 Å structure (the orthorhombic crystal form) are colored magenta, cyan and red. RsiG and σ^{WhiG} are labelled as is the c-di-GMP dimer bound between the proteins. All heterodimeric complexes are identical. Also, note, each c-di-GMP dimer adopts an identical conformation when bound to the RsiG-σ^{WhiG} complex.

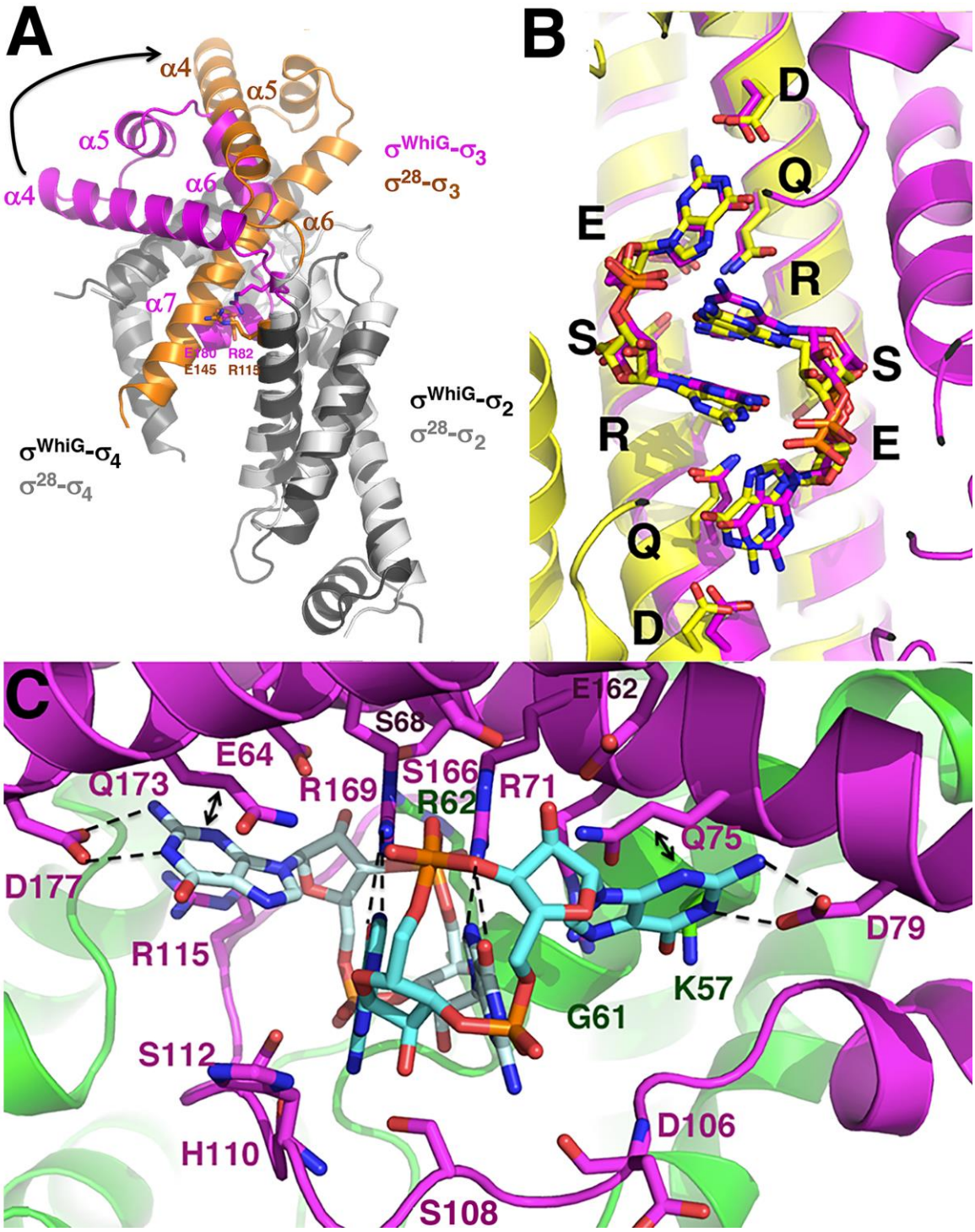

Figure S3. Characterization of RsiG and σ^{WhiG} structure and detailed interactions, related to Figure 5. (A) Overlay of the RsiG bound σ^{WhiG} structure onto the FlgM bound σ^{28} structure (Sorenson et al., 2004). σ domains 2 and 4 are colored grey and black for σ^{28} and σ^{WhiG}, respectively. These domains overlay as a unit while the σ_3 regions (colored orange and magenta σ^{28} and σ^{WhiG}, respectively) do not. Nonetheless a salt bridge is conserved between a conserved glutamate in σ_3 and conserved arginine in σ_2 of both proteins. (B) Superimposition of two RsiG structures whereby one $E(X)_3S(X)_2R(X)_3Q(X)_3D$ repeat motif of one structure (magenta) was overlaid onto the second repeat of the other structure (yellow). The remaining helices and motifs of the two structures also superimpose as do the c-di-GMP dimers. (C) Detailed c-di-GMP interactions with RsiG and σ^{WhiG}. All residues that contact c-di-GMP are shown in the figure. H-bonds are indicated by dashed lines.

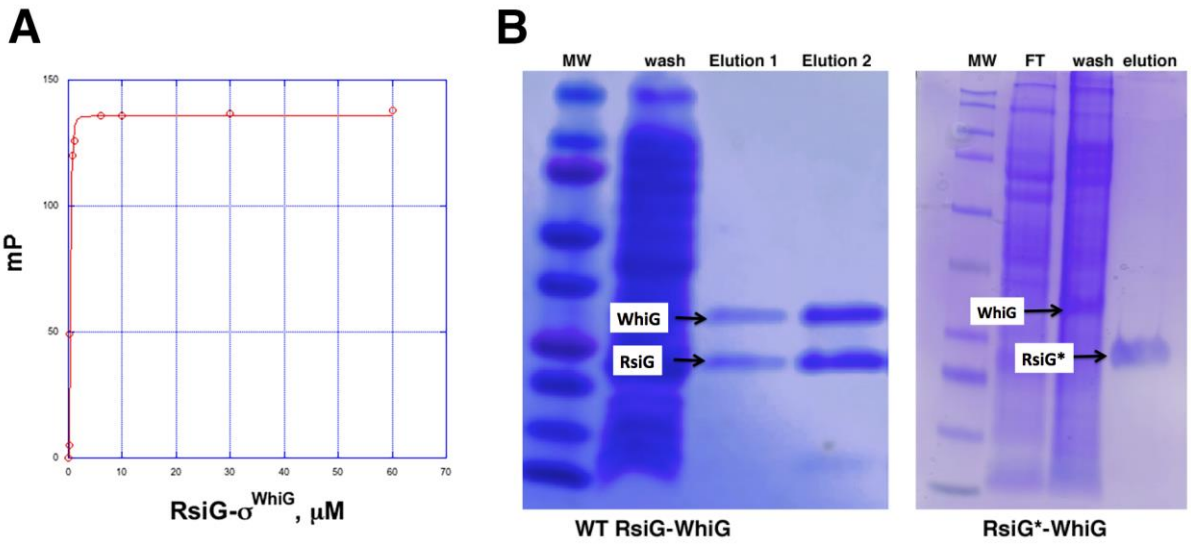

Figure S4. c-di-GMP binds with high affinity to RsiG- RsiG-σ^{WhiG} and is required for stable RsiG-σ^{WhiG} complex formation, related to Figure 7. (A) FP binding isotherm of the interaction between F-c-di-GMP and a solution with equimolar RsiG and σ^{WhiG}. The resultant K_d is 0.39 ± 0.05 μM. This experiment was repeated three times (technical replicates). (B) Coexpression of σ^{WhiG} with WT his_6-RsiG (left) or his_6-RsiG* (right). The positions of the proteins on the gel are labelled and, as can be observed, σ^{WhiG} copurifies with WT his_6-RsiG but not with his_6-RsiG*.

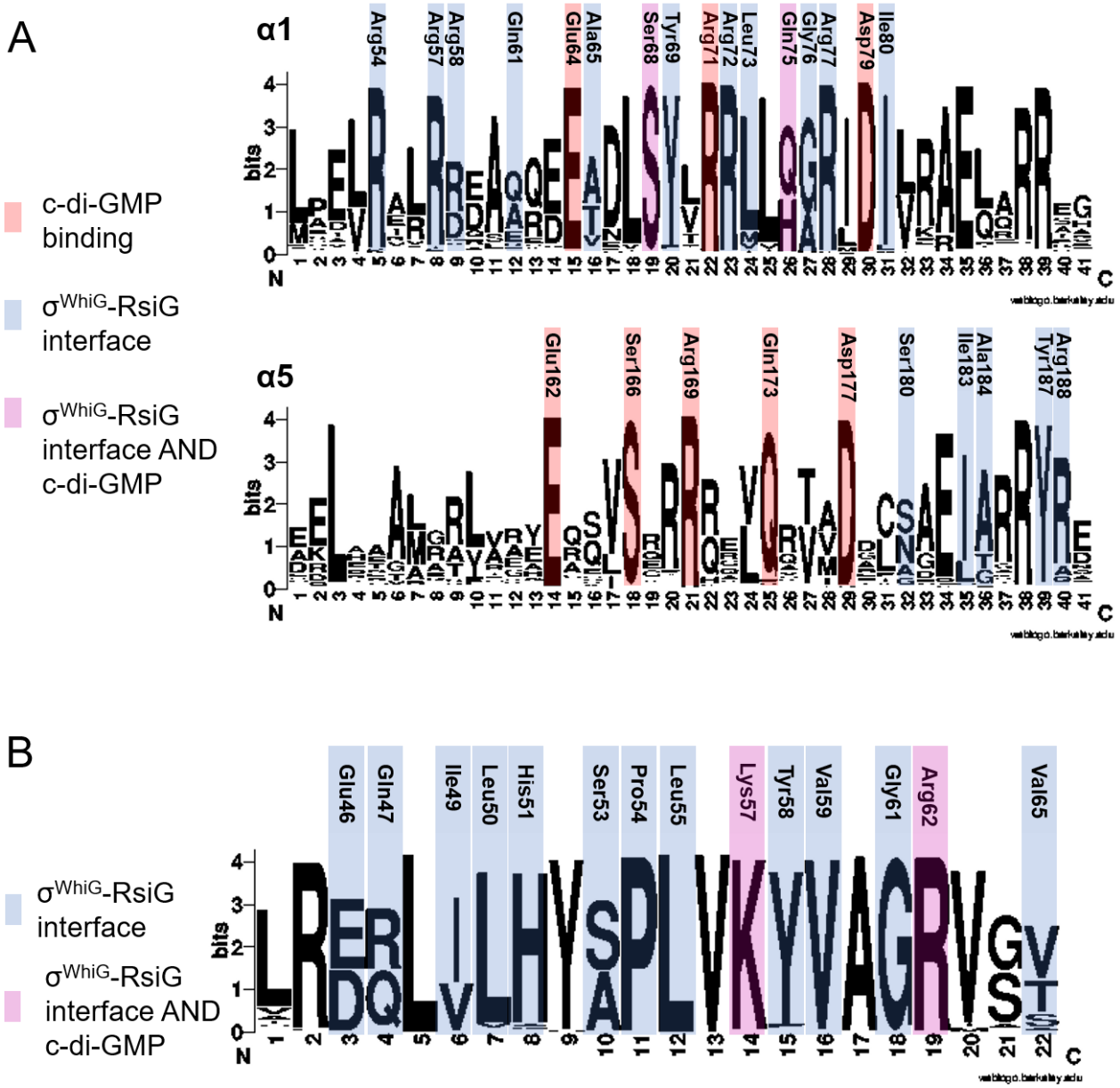

Figure S5. Conservation of residues in RsiG and σ^{WhiG} involved in binding c-di-GMP, related to Figure 7. (A) Sequence logos depicting amino acid sequence conservation of the two alpha helices involved in c-di-GMP binding among RsiG homologs in all bacteria. Residues involved in the σ^{WhiG}-RsiG interface and/or c-di-GMP binding are indicated. Note the conservation of the two $E(X)_3S(X)_2R(X)_3Q(X)_3D$ signature c-di-GMP-binding motifs. Residues are numbered based on the *S. venezuelae* sequence. RsiG homologs were identified by a reciprocal BLAST search (e-value cut off = 0.001) of the 3,962 'reference' or 'representative' annotated genomes available at GenBank, using the *S. venezuelae* RsiG sequence as a query. Homologs were aligned using MUSCLE (Edgar 2004). Fourteen sequences (all <41% sequence identity) that did not align well were removed from the analysis. The remaining 134 sequences were re-aligned, the regions of interest extracted, and the resulting alignments were used to create Weblogos (Crooks et al., 2004). (B) Sequence logo depicting amino acid sequence conservation of σ region 2.1 among σ^{WhiG} homologs that co-occur with RsiG. Residues involved in the σ^{WhiG}-RsiG interface and/or c-di-GMP binding are indicated. Note that the two σ^{WhiG} residues that make direct contacts to c-di-GMP, Lys57 and Arg62, are highly conserved. Residues are numbered based on the *S. venezuelae* sequence. Homologs were identified by a reciprocal BLAST search of the 134 genomes that contain a *rsiG* homolog, using the *S. venezuelae* σ^{WhiG} sequence as a query. The sequences were aligned using MUSCLE (Edgar 2004), σ region 2.1 was extracted and the resulting alignment used to create a Weblogo (Crooks et al., 2004).

Table S1: Data collection and refinement statistics for RsiG-σ^{WhiG} structures, related to Figures 5 and 6

Structure	form 1:RsiG-σ^{WhiG}	form 2:RsiG-σ^{WhiG}
PDB code	6PFJ	6PFV
Space group	$P6_4$	$P22_12_1$
Cell constants (Å)	a=b=92.1,c=96.6	a=79.8, b=97.3, c=204.6
Cell angles (º)	$\alpha=\beta=90.0$, $\gamma=120.0$	$\alpha=\beta=\gamma=90.0$
Resolution (Å)	79.8-2.08	87.9-3.00
R_{sym}(%)[a]	5.1 (86.9)[b]	9.8 (99.8)
R_{pim} (%)	1.4 (62.4)	5.3 (65.3)
Overall I/σ(I)	20.5 (1.4)	8.9 (1.2)
#Unique Reflections	53900	32724
#Total Reflections	410742	132151
% Complete	96.2 (94.0)	99.1 (99.1)
CC(1/2)	1.00 (0.537)	0.997 (0.447)
Multiplicity	7.1 (7.0)	4.0 (4.2)
Refinement Statistics		
Resolution (Å)	79.8-2.08	87.9-3.00
R_{work}/R_{free}(%)[c]	19.5/23.8	20.9/27.9
Rmsd		
Bond angles (º)	1.38	0.855
Bond lengths (Å)	0.004	0.004
Ramachandran analysis		
Favored (%/)	97.8	91.0
Disallowed(%)	0.0	0.0

[a] $R_{sym} = \Sigma\Sigma|Ihkl-Ihkl(j)|/ \Sigma Ihkl$, where Ihkl(j) is observed intensity and Ihkl is the final average value of intensity. [b] values in parentheses are for the highest resolution shell. [c] $R_{work} = \Sigma||Fobs| - |Fcalc||/\Sigma|Fobs|$ and $R_{free} = \Sigma||Fobs| - |Fcalc||/\Sigma|Fobs|$; where all reflections belong to a test set of 5% randomly selected data.

Table S2. Distribution of *rsiG* homologs in bacterial families, related to Figures 4, 5 and 6

Family	Number of *rsiG* homologs identified	Number of genomes in search set
Acidimicrobiaceae	2	3
Acidothermaceae	1	1
Actinopolysporaceae	2	2
Catenulisporaceae	1	1
Cellulomonadaceae	1	8
Conexibacteraceae	1	1
Cryptosporangiaceae	1	2
Geodermatophilaceae	16	16
Ilumatobacteraceae	1	1
Kineosporiaceae	1	1
Nocardioidaceae	1	19
Patulibacteraceae	1	1
Pseudonocardiaceae	39	46
Rubrobacteraceae	2	2
Streptomycetaceae	63	63
Thermoleophilaceae	1	1

Table S3. Primers, plasmids, and strains used in this study, related to STAR Methods

Primers	5' sequence
vnz26215_redi_F	GACCGCGCTGCGGTGCCCCCAGCAGCCCGGGGCACCGTGATTCCGGGGATCCGTCGACC
vnz26215_redi_R	TGGGCACGGCTCCACTGTACGACCGGCTCGCCCCGGTCATGTAGGCTGGAGCTGCTTC
vnz15005_redi_F	GGCGTCCGAAAGCCGGCGGAGGAAAGGAGCATGTGCATGATTCCGGGGATCCGTCGACC
vnz15005_redi_R	TCGTCTCATGCGGTCATGGCCTCATGGCCCATGGCCTCATGTAGGCTGGAGCTGCTTC
vnz19430_redi_F	CGGTGCGCCTCCGCACCGGTCGAGGGGACGAATCTGATGATTCCGGGGATCCGTCGACC
vnz19430_redi_R	ACCCGCACGCGAGTTTTTCCGGGCGCCGGGCCGCCGTCATGTAGGCTGGAGCTGCTTC
vnz26215_check_F	CGCATGCCCCAGCACACC
vnz26215_check_R	CTGCATCGTCCGGTGCTC
vnz15005_check_F	CGATCCGATGATCCGATCGGA
vnz15005_check_R	GTCGTCGATCCCCAGGTGA
vnz19430_check_F	TGCACCACTGCACGCATGC
vnz19430_check_R	GCTGCCAGTCGGGGAACTC
vnz26215_comp_F	GGCGAAGCTTCCTGGAGCATTCGGGTGA
vnz26215_comp_R	GGGGTACCGGTGCTCGGCCACCGAG
vnz19430_comp_F	GGCGAAGCTTACCCTCTGCACCACTGCAC
vnz19430_comp_R	GGGGTACCCATCCTCCGACCCTACGCAG
vnz26215_ermE_F	GGGAATTCCATATGCCCCAGCACACCTCCG
vnz26215_ermE_R	GGAAGCTTGGTGCTCGGCCACCGAG
HI_ermE_P1	GTCTAGAACAGGAGGCCCCATATGAGTACCCTTGCGCACACCATG
HI_ermE_P2	TTACCTCCGATGTTGAGTCAGTGTTCGCGGGGGGC
HI_ermE_P3	CGAACACTGACTCAACATCGGAGGTAAGCCATGTCCGTTCTCCTCGAG
HI_ermE_P4	TGAGAACCCTAGGGGATCCAAAGCTTTCAGTGGATGATC
vnz28820_qRT_F	CGGGAGGTCGAGGTGCTCAG
vnz28820_qRT_R	TGGCTCTTCACGGTGAGGGC
hrdBqRT_F	TGTTCTGCGCAGCCTCAATC
hrdBqRT_R	CTCTTCGCTGCGACGCTCTT
vnz26215_BACTH_F	CTAGTCTAGAGATGCCCCAGCACACCTCCG
vnz26215_BACTH_R	GGGGTACCCGGCGTCCGACGTCGGCCA
T18seq_F	GTGTGGAATTGTGAGCGGAT
T18seq_R	TTCCACAACAAGTCGATGCG
T25seq_F	CGGTGACCAGCGGCGATT
T25seq_R	GGCGATTAAGTTGGGTAACGCC
NT25seq_F	CCCCAGGCTTTACACTTTATGC
NT25seq_R	TTGATGCCATCGAGTACGGCT
T18Cseq_F	GTGCCGAGCGGACGTTCGA
T18Cseq_R	CTTAACTATGCGGCATCAGAGC
vnz19430_BACTH_F	GGGGTACCCGGGCGAGCAGGTCGTCGAC
vnz19430_BACTH_R	CTAGTCTAGAGATGAGTGCACCTGGCACCGG
vnz26215_MCS1_F	CCGGAATTCGATGCCCCAGCACACCTCCG
vnz26215_MCS1_R	CCCAAGCTTTCAGCGTCCGACGTCGGC
vnz19430_MCS2_F	GGGAATTCCATATGAGTGCACCTGGCACCGG
vnz19430_MCS2_R	GGGGTACCTCAGGCGAGCAGGTCGTCG

Plasmid	Relevant genotype/comments	Source
pIJ790	Modified l RED recombination plasmid [*oriR101*] [*repA101*(ts)] *araBp-gam-be-exo*	Gust et al., 2003
pIJ773	Plasmid template for amplification of the apr oriT cassette for 'Redirect' PCR-targeting	Gust et al., 2003
pIJ10770	Plasmid cloning vector for the conjugal transfer of DNA from *E. coli* to *Streptomyces* spp. Integrates site specifically at the ΦBT1 attachment site (Hyg^R).	Schlimpert et al., 2017
pIJ10900	pIJ10770 carrying *whiG* driven from its own promoter	This work
pIJ10901	pIJ10770 carrying *rsiG* driven from its own promoter	This work
pIJ10913	pIJ10770 carrying *rsiG** driven from the WT *rsiG* promoter	
pIJ10257	Plasmid cloning vector for the conjugal transfer of DNA (under control of the ermE* constitutive promoter) from *E. coli* to *Streptomyces* spp. Integrates site specifically at the ΦBT1 attachment site (Hyg^R).	Hong et al., 2005
pIJ10902	pIJ10257 carrying *whiG*, driven by ermE*	This work
pIJ10906	pIJ10257 carrying *whiH* and *whiI*, driven by ermE*	This work
pKT25	Two-hybrid plasmid, N-terminal cyaAT25 fusion (Kan^R)	Karimova et al., 1998
pKNT25	Two-hybrid plasmid, C-terminal cyaAT25 fusion (Kan^R)	Karimova et al., 1998
pUT18	Two-hybrid plasmid, C-terminal cyaAT18fusion (Amp^R)	Karimova et al., 1998

Plasmid	Relevant genotype/comments	Source
pUT18C	Two-hybrid plasmid, N-terminal cyaAT18fusion (Amp^R)	Karimova et al., 1998
pKT25-zip	A derivative of pKT25 in which the leucine zipper of GCN4 is genetically fused in frame to the T25 fragment	Karimova et al., 1998
pUT18C-zip	A derivative of pUT18C in which the leucine zipper of GCN4 is genetically fused in-frame to the T18 fragment	Karimova et al., 1998
pIJ10907	pKT25 carrying *whiG*	This work
pIJ10908	pKNT25 carrying *whiG*	This work
pIJ10909	pUT18 carrying *whiG*	This work
pIJ10910	pUT18C carrying *whiG*	This work
pIJ10911	pKT25 carrying *rsiG*	This work
pIJ10912	pUT18 carrying *rsiG*	This work
pCOLADuet-1	Expression vector for coexpression of two target genes, each under the control of a T7 promoter (Kan^R)	Novagen
pET15B	T7 expression vector (Amp^R)	Novagen
pIJ10914	pCOLADuet-1 carrying *whiG* at MCS1 and *rsiG* at MCS2	This work
pIJ10915	pCOLADuet-1 carrying Δ26 *rsiG* at MCS1 and *whiG* at MCS2 (genes codon optimized for *E. coli*)	This work
pIJ10916	pCOLADuet-1 carrying Δ26 *rsiG** at MCS1 and *whiG* at MCS2 (genes codon optimized for *E. coli*)	This work
pIJ10917	pCOLADuet-1 carrying *rsiG* at MCS1	This work
pIJ10918	pET15B carrying *rsiG** (gene codon optimized for *E. coli*)	This work
pIJ10919	pCOLADuet-1 carrying Δ26 *rsiG*(L56M-L85M) at MCS1 (gene codon optimized for *E. coli*)	This work
pIJ10920	pCOLADuet-1 carrying *whiG* at MCS1 (gene codon optimized for *E. coli)*	This work
pKF351	Plasmid cloning vector for the conjugal transfer of DNA from *E. coli* to *Streptomyces* spp. Integrates site specifically at the ΦC31 attachment site (Hyg^R) and carries *ftsZ-ypet* driven from its own promoter.	Schlimpert et al., 2017
pSS5	Plasmid cloning vector for the conjugal transfer of DNA from *E. coli* to *Streptomyces* spp. Integrates site specifically at the ΦBT1 attachment site (Hyg^R) and carries *ftsZ-ypet* driven from its own promoter.	Schlimpert et al., 2017

Strains	Relevant genotype/notes	Reference
S. venezuelae		
ATCC10712	wild type	
SV6	*ΔwhiG::apr*	This work
SV80	*Δvnz15005::apr*	This work
SV81	*ΔrsiG::apr*	This work
SV6-pIJ10770	*ΔwhiG::apr* with pIJ10770 integrated at the ΦBT1 attachment site	This work
SV6-pIJ10900	*ΔwhiG::apr* with pIJ10900 integrated at the ΦBT1 attachment site	This work
Sven-pIJ10257	wild type with pIJ10257 integrated at the ΦBT1 attachment site	This work
Sven-pIJ10902	wild type with pIJ10902 integrated at the ΦBT1 attachment site	This work
SV6-pIJ10257	*ΔwhiG::apr* with pIJ10257 integrated at the ΦBT1 attachment site	This work
SV6-pIJ10906	*ΔwhiG::apr* with pIJ10906 integrated at the ΦBT1 attachment site	This work
SV81-pIJ10770	*ΔrsiG::apr* with pIJ10770 integrated at the ΦBT1 attachment site	This work
SV81-pIJ10901	*ΔrsiG::apr* with pIJ10901 integrated at the ΦBT1 attachment site	This work
SV81-pIJ10913	*ΔrsiG::apr* with pIJ10913 integrated at the ΦBT1 attachment site	This work
Sven-pIJ10257-pKF351	wild type with pIJ10257 integrated at the ΦBT1 attachment site and pKF351 integrated at the ΦC31 attachment site	This work
Sven-pIJ10902-pKF351	wild type with pIJ10902 integrated at the ΦBT1 attachment site and pKF351 integrated at the ΦC31 attachment site	This work
SV81-pSS5	*ΔrsiG::apr* with pSS5 integrated at the ΦBT1 attachment site	This work
E. coli		
DH5α	F– ϕ80*lac*ZΔM15 Δ(*lac*ZYA-*arg*F)U169 *rec*A1 *end*A1 *hsd*R17(rK–, mK+) *pho*A *sup*E44 λ– *thi*-1 *gyr*A96 *rel*A1	Invitrogen
ET12567(pUZ8002)	ET12567 containing helper plasmid pUZ8002	Paget et al., 1999
BW25113	Δ(*araD-araB*)*567* Δ*lacZ4787*(::*rrnB-4*) *lacIp-4000*($lacI^Q$), λ−*rpoS369*(*Am*) *rph-1*Δ(*rhaD-rhaB*)*568 hsdR514*	Datsenko and Wanner 2000
BTH101	F– *cya-99 araD139 galE15 galK16 rpsL1 (Strr) hsdR2 mcrA1 mcrB1*	Karimova et al., 1998
BL21 pLysS Rosetta	F– *ompT hsd*S(rB- mB-) *gal dcm* (DE3) pLysSRARE (Cam^R)	Novagen